CrystEngComm

PAPER

View Article Online
View Journal | View Issue

Cite this: *CrystEngComm*, 2014, **16**, 1359

Crystal engineering with coordination compounds of 2,6-dicarboxy-4-hydroxypyridine and 9-aminoacridine fragments driven by different nature of the face-to-face π···π stacking†

Hossein Eshtiagh-Hosseini,[a] Masoud Mirzaei,*[a] Sara Zarghami,[a] Antonio Bauzá,[b] Antonio Frontera,*[b] Joel T. Mague,[c] Morteza Habibi[d] and Mojtaba Shamsipur[d]

Received 28th August 2013,
Accepted 6th November 2013

DOI: 10.1039/c3ce41730a

www.rsc.org/crystengcomm

(H9a-Acr)$_2$[Ni(hypydc)$_2$]·4H$_2$O (**1**), (H9a-Acr)$_2$[Co(hypydc)$_2$]·3H$_2$O (**2**), (H9a-Acr) [Cr(hypydc)$_2$]·3H$_2$O (**3**), and (H9a-Acr)$_2$[Cd(hypydc)$_2$]·3H$_2$O (**4**) compounds (H$_2$hypydc = 2,6-dicarboxy-4-hydroxypyridine or chelidamic acid; 9a-Acr = 9-aminoacridine) were synthesized *via* proton transfer and characterised by elemental analysis, IR spectroscopy, and single crystal X-ray diffraction techniques. Thermogravimetric analysis (TGA) was carried out on compounds **1** and **2**. Compounds **1**–**4** have distorted octahedral geometries with two hypydc^{2-} ions coordinated as tridentate ligands to each metal ion through one oxygen atom of each carboxylate group and the nitrogen atom of the pyridine ring. In the compounds, strong hydrogen bonds between anionic, cationic, and water fragments and especially the different natures of the $\pi^{+}\cdots\pi^{-}$ and $\pi^{-}\cdots\pi^{-}$ stacking interactions play important roles in the construction of three-dimensional supramolecular frameworks which have been analysed in detail. The smaller *trans* N–M–N angle observed in **3** as compared with the others has been analysed using DFT calculations. Solution studies have also been performed to understand the behaviour of the ternary systems M^{n+} –H$_2$hypydc–9a-Acr in aqueous solution.

1. Introduction

'One of the most general and important reactions in chemistry'[1] has been defined as the reaction which involves the transfer of a proton from one atom to another. The proton transfer belongs to the class of simplest chemical reactions that are very important in many physical, biochemical, and technological processes, acid–base neutralization, electrophilic addition, enzyme mechanisms, contributing to the catalytic power of enzymes *etc.*, and thus selected simple hydrogen bonded systems are reasonable models to study this phenomenon.[2–4] Recently, a large number of theoretical and experimental studies have been carried out to enrich the information regarding the possible mechanisms of proton-transfer, tautomeric equilibria, and relevant properties associated with proton-transfer processes.[5] Water-soluble, pharmaceutically important carboxylic acids or amine salts and some ionic liquids are examples for which proton transfer strategy is utilized.[6] Derivatives of carboxylic acids occupy a very particular place in this research field so that recently many metal complexes with these ligands have been synthesized and characterized by different research groups. As a multicarboxylate and N-heterocyclic ligand, chelidamic acid (2,6-dicarboxy-4-hydroxypyridine, H$_2$hypydc) has been of great interest due to its usage in many areas of science, such as proton transfer reactions, coordination chemistry, biochemistry, organic chemistry, medical chemistry, and even in HIV investigation.[7] These characteristics make it an appealing candidate for the production of proton transfer compounds and interesting structural motifs. Up to now, several transition-metal complexes based on chelidamic acid have been documented, many of them containing lanthanide metals.[8–22] At the initiation of this work, to the best of our knowledge, no proton transfer studies and complexes using this ligand with 9-aminoacridine had been reported (however as the study was being completed, three such complexes were reported, one of which is identical with the nickel complex prepared here).[20] Therefore, we selected chelidamic acid

[a] *Department of Chemistry, Ferdowsi University of Mashhad, Mashhad 917751436, Iran. E-mail: mirzaeesh@um.ac.ir*
[b] *Departament de Quimica, Universitat de les Illes Balears, (Baleares), Palma de Mallorca, Spain. E-mail: toni.frontera@uib.es*
[c] *Department of Chemistry, Tulane University, New Orleans, LA 70118, USA*
[d] *Department of Chemistry, Razi University, Kermanshah, Iran*

† Electronic supplementary information (ESI) available: CCDC 940542–940545 contains the supplementary crystallographic data for 1–4, respectively. For ESI and crystallographic data in CIF or other electronic format see DOI: 10.1039/c3ce41730a

as the major ligand and 9-aminoacridine as an auxiliary (see Scheme 1) ligand for testing their reactions with some transition metal salts. As a result, we have synthesized and X-ray characterized four proton transfer complexes: (H9a-Acr)$_2$[Ni(hypydc)$_2$]·4H$_2$O (**1**), (H9a-Acr)$_2$[Co(hypydc)$_2$]·3H$_2$O (**2**), (H9a-Acr)[Cr(hypydc)$_2$]·3H$_2$O (**3**), and (H9a-Acr)$_2$[Cd(hypydc)$_2$]·3H$_2$O (**4**). In all these structures, there are strong hydrogen bonds as well as non-covalent interactions such as π···π, O–H···π, C–H···π and various heterosynthons, which create interesting 3-D supramolecular structures.

2. Experimental

2.1. Chemicals and methods

2,6-Dicarboxy-4-hydroxypyridine (98%), 9-aminoacridine (99%), Ni^{II} chloride hexahydrate (99%), Co^{II} nitrate hexahydrate (99%), Cr^{III} chloride hexahydrate (99%), and Cd^{II} nitrate tetrahydrate (99%), were purchased from Merck company and used without further purification. Infrared spectra (4000–600 cm^{-1}) were recorded on a Buck 500 scientific spectrometer as KBr discs. Elemental analyses (C, H, and N contents) were carried out on a Thermo Finnigan Flash model 1112 EA microanalyzer. Thermal gravimetric analyses (TGA) were carried out in an air atmosphere between 20 and 950 °C at a heating rate of 10 °C min^{-1} on a Shimadzu Japan TGA-50 (see Fig. S1–S2†). The X-ray data were obtained with a Bruker Smart APEX diffractometer.

2.2. Syntheses of complexes 1–4

2.2.1 (H9a-Acr)$_2$[Ni(hypydc)$_2$]·4H$_2$O (1). A solution of 9a-Acr (29.0 mg, 0.1 mmol) in methanol was added to an aqueous solution of chelidamic acid (30.0 mg, 0.1 mmol). The mixture was refluxed for 1 h at 65 °C after which an aqueous solution of Ni^{II} chloride hexahydrate (20.0 mg, 0.08 mmol) was added and the refluxing continued for 3 h. Green crystals were obtained by slow evaporation of the reaction mixture at room temperature (m.p. >300 °C). Elemental analysis: anal. calc. for $C_{40}H_{36}N_6NiO_{14}$: C, 54.33; H, 4.07; N, 9.51. Found: C, 54.18; H, 4.11; N, 9.60%. IR bands (KBr pellet, cm^{-1}): 3375, 3190, 3114, 3062, 2962, 2853, 2720, 2616, 2516, 1624, 1591, 1482, 1377, 1296, 1168, 1116, 1045, 941, 865, 793, 746.

2.2.2 (H9a-Acr)$_2$[Co(hypydc)$_2$]·3H$_2$O (2). The synthetic procedure for **2** was similar to that for **1**, but using Co^{II} nitrate hexahydrate (22.0 mg, 0.075 mmol) in place of Ni^{II} chloride hexahydrate. Orange crystals were obtained by slow evaporation of the reaction mixture at room temperature (m.p. >300 °C). Elemental analysis: anal. calc. for $C_{40}H_{34}CoN_6O_{13}$: C, 55.45; H, 3.93; N, 9.70. Found: C, 56.11; H, 4.00; N, 9.38%. IR bands (KBr pellet, cm^{-1}): 3390, 3126, 2923, 2839, 2688, 1818, 1592, 1474, 1366, 1305, 1239, 1178, 1107, 1036, 938, 806, 745.

2.2.3 (H9a-Acr)[Cr(hypydc)$_2$]·3H$_2$O (3). The synthesis of **3** was similar to that for **1**, but with Cr^{III} chloride hexahydrate (20.0 mg, 0.074 mmol) in place of Ni^{II} chloride hexahydrate. Dark green crystals were obtained by slow evaporation of the reaction mixture at room temperature (m.p. >300 °C). Elemental analysis: anal. calc. for $C_{27}H_{21}CrN_4O_{14}$: C, 47.83; H, 3.12; N, 7.12. Found: C, 47.63; H, 3.35; N, 7.42%. IR bands (KBr pellet, cm^{-1}): 3364, 3249, 3138, 3061, 2740, 2615, 2514, 1664, 1606, 1496, 1481, 1363, 1275, 1169, 1112, 1063, 929, 876, 800, 756, 689, 660.

2.2.4 (H9a-Acr)$_2$[Cd(hypydc)$_2$]·3H$_2$O (4). The synthesis of **4** was similar to that for **1**, but with Cd^{II} nitrate tetrahydrate (23.0 mg, 0.075 mmol) in place of Ni^{II} chloride hexahydrate. Orange crystals were obtained by slow evaporation of the reaction mixture at room temperature (m.p. >300 °C). Elemental analysis: anal. calc. for $C_{40}H_{36}CdN_6O_{14}$: C, 51.22; H, 3.84; N, 8.96. Found: C, 52.00; H, 3.69; N, 8.72%. IR bands (KBr pellet, cm^{-1}): 3488, 3375, 3297, 3128, 3056, 2922, 2777, 2693, 2577, 2495, 1797, 1777, 1645, 1589, 1489, 1427, 1346, 1252, 1176, 1111, 1027, 978, 891, 803, 750, 692.

2.3. X-ray crystallography

Full spheres of data for **1–4** were collected by a combination of φ and ω scans using narrow (0.3–0.5°) frames on a Bruker-AXS Smart APEX diffractometer under control of the APEX2[23] program suite. Raw intensities were converted to F^2 values by SAINT[24] which also provided final unit cell dimensions from the least-squares refinement of *ca.* 9000 reflections drawn from the full data set. Corrections for absorption and merging of equivalent reflections were performed with SADABS,[25] the structures solved by direct methods (SHELXS)[26] and refined by full-matrix, least-squares procedures (SHELXL).[26] H-atoms attached to carbon were placed in calculated positions while the remainder were placed in positions derived from difference Fourier syntheses. All were included as riding contributions with isotropic displacement parameters tied to those of the attached atoms.

2.4. Theoretical methods

The energies of all compounds included in this study were computed at the BP86-D3/def2-TZVPD level of theory within the program TURBOMOLE version 6.4.[27] For the calculations we have used the BP86 functional with the latest available correction for dispersion (D3).[28] We have used the crystallographic coordinates to perform the calculations.

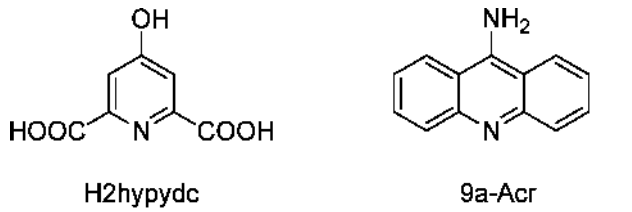

H2hypydc 9a-Acr

Scheme 1 2,6-Dicarboxy-4-hydroxypyridine (left) and 9-aminoacridine (right) ligands used in this work. Their acronyms used throughout this manuscript are also indicated.

2.5. Potentiometric pH titrations

All potentiometric pH measurements were carried out on a model 686 digital pH meter equipped with a combined glass–calomel electrode. The base used for potentiometric pH titrations was carbonate-free lithium hydroxide, which was standardized against primary standard oven-dried potassium hydrogen phthalate. A CO_2-free atmosphere for the base was ensured throughout. The potentiometric apparatus used consisted of a 50 mL glass jacketed cell, a constant temperature bath (MLW thermostat, 25.0 ± 0.1 °C), a combined glass electrode and a 10 mL capacity Metrohm piston burette, for which the tip was sealed in the cap of the titration cell with a clamp and O-rings. Atmospheric CO_2 was excluded from the titration cell with a purging stream of purified nitrogen gas. The electrodes were calibrated in the thermostated cell with standard acid–base to read pH directly. The value of $K_{SH} = [H^-][OH^-]$, for a 50% methanol–50% water mixture, used in the calculations was $10^{-16.70}$. The concentrations of chelidamic acid (H_2hypydc, L) and 9-aminoacridine (9a-Acr, Q) were 1.27×10^{-3} M. A standard carbonate-free 0.059 M lithium hydroxide solution was used in all titrations. The ionic strength was adjusted to 0.1 M with $NaNO_3$. Before an experimental point (pH) was measured, sufficient time was allowed for establishment of equilibrium. Ligand protonation constants and their metal complexes protonation, stability and hydrolysis constants were calculated using the program BEST described by Martell and Motekaitis.[29–31]

3. Results and discussion

3.1. Syntheses and IR

All four proton transfer complexes were obtained by using similar methods and conditions. The infrared spectra and elemental analyses of **1–4** are fully consistent with their structural characteristics as determined by single-crystal X-ray diffraction. As expected, the IR spectra were nearly the same and show vibrations due to the water, carboxylic acid, and amine fragments. Absorptions in the range 3500–3100 cm^{-1} correspond to the N–H and O–H stretching vibrations of the amino groups and water molecules respectively. Strong characteristic bands of the carboxyl groups are observed in the range 1665–1590 cm^{-1} for the asymmetric vibrations and 1375–1350 cm^{-1} for symmetric vibrations, respectively. The separation between $\nu_{as}(COO^-)$ and $\nu_s(COO^-)$ has been often used to diagnose the coordination modes in the carboxylate ligands. The separation for unidentate carboxylato groups is > 200 cm^{-1}, whereas it is < 200 cm^{-1} in bidentate ones.[32] Thus, the separation of > 200 cm^{-1} in **1–4** indicates a unidentate coordination mode for the carboxylate groups. The absence of the characteristic bands at around 1700 cm^{-1} attributed to the carboxyl groups indicates that complete deprotonation of all carboxylate groups in **1–4** has occurred upon reaction with metal ions. The weak bands which appear in the range 745–755 cm^{-1} can be attributed to an in-plane vibration of the OCO group.

3.2. Thermal behaviors of 1 and 2

The TG–DTA–DTG curves of **1** are shown in Fig. S1.† The peak at 127 °C corresponds to the loss of four water molecules (found 8.14, calcd. 8.17%). The second stage is related to the removal of chelidamic acid at 372 °C (found 41.45, calcd. 40.72%). The last stage corresponds to the decomposition of the 9-aminoacridinium cations at 420 °C (found 42.71, calcd. 43.75%).The TG curves of **2** are shown in Fig. S2.† The peak at 177 °C corresponds to the loss of four water molecules (found 6.23, calcd. 6.24%). The second stage is related to the removal of chelidamic acid at 350 °C (found 42.31, calcd. 40.47%). The last stage corresponds to the decomposition of the 9-aminoacridinium cations at 420 °C (found 44.87, calcd. 42.33%).

3.3. Structure descriptions

The crystallographic data for compounds **1–4** are shown in Table 1 while selected bond lengths, bond angles, and torsion angles are given in Table 2. Hydrogen bond geometries of the four compounds are shown in Table 3. Overall, the four complexes display considerable similarities with each metal ion being chelated by two tridentate hypydc ligands which are approximately orthogonal to one another to yield distorted octahedral coordination spheres. Considering that both nitrogen atoms are located at the apical positions, the basal plane is formed by the four oxygen atoms, which exhibit a tetrahedral distortion as a result of the geometric constraints of the hypydc ligands (see Table 2 for the *trans* O–M–O angles). The structures are completed by 9-aminoacridinium cations protonated at the pyridine nitrogen and lattice water molecules. Strong O–H···O, N–H···O, and several aromatic π···π interactions serve to tie all components together.

3.3.1. Crystal structure of $(H9a\text{-}Acr)_2[Ni(hypydc)_2]\cdot 4H_2O$ (1). The asymmetric unit of **1** is shown in Fig. 1 together with the atomic numbering scheme while selected bond length and angles appear in Table 2. Two hypydc units coordinate to the Ni^{II} atom in a nearly perpendicular fashion as indicated by the *trans* N(1)–Ni(1)–N(2) angle of 176.48(6)° and the angle between the mean planes containing Ni(1), O(1), C(1), C(2), N(1), C(6), C(7), O(3) and Ni(1), O(6), C(8), C(9), N(2), C(13), C(14), O(8) of 84.90(4)°. The O_4N_2 environment about nickel has axial positions occupied by the nitrogen atoms of the aromatic ligand with short Ni–N distances, 1.9685(16) and 1.9636(15) Å and the equatorial sites occupied by O(1), O(3), O(6) and O(8) of the carboxylate groups at distances 2.1449(14), 2.1188(15), 2.1226(14), and 2.1419(14) Å respectively. The tetrahedral distortion of these four atoms is indicated by the O(1)–Ni(1)–O(3) and O(6)–Ni(1)–O(8) angles which are 154.79(5)° and 155.36(5)° respectively. In addition, the asymmetric unit contains two protonated 9-aminoacridine molecules that are arranged in an antiparallel stacking mode and four water molecules, one of which is disordered over two adjacent sites. This last is not surprising considering the number of suitably-sized voids in the structure and the

Table 1 Crystallographic data for 1–4

	1	2	3	4
Empirical formula	$C_{40}H_{36}N_6NiO_{14}$	$C_{40}H_{34}CoN_6O_{13}$	$C_{27}H_{21}CrN_4O_{14}$	$C_{40}H_{36}CdN_6O_{14}$
Formula weight	883.46	865.66	677.48	937.15
Temperature/K	100(2)	100(2)	100(2)	100(2)
Crystal system	Triclinic	Monoclinic	Triclinic	Triclinic
Space group	$P\bar{1}$	$P2_1/c$	$P\bar{1}$	$P\bar{1}$
a (Å)	11.8637(16)	10.574 (3)	7.8867 (12)	12.0580(12)
b (Å)	13.8353(18)	23.672 (6)	11.0204 (17)	13.9067(14)
c (Å)	14.0619(18)	14.903 (4)	16.859 (3)	14.0032(15)
α (°)	111.781(1)	90	84.453 (2)	111.967(1)
β (°)	113.229(1)	104.379	89.358 (2)	115.126(1)
γ (°)	92.745(2)	90	75.087 (2)	94.003(2)
Volume (Å^3)	1917.9(4)	3613.6(16)	1409.2(4)	1897.1(3)
Z	2	4	2	2
Density (calculated)	1.53	1.591	1.597	1.641
Absorption coefficient (mm^{-1})	0.587	0.557	0.488	0.657
F(000)	916	1788	694	956
Crystal size (mm^3)	0.21 × 0.18 × 0.11	0.28 × 0.14 × 0.04	0.21 × 0.15 × 0.13	0.31 × 0.23 × 0.22
Θ range for data collection	1.63 to 28.53°	2.17 to 28.41°	2.17 to 29.12°	1.89 to 29.14°
Index ranges	$-15 \le h \le 15$	$-14 \le h \le 14$	$-10 \le h \le 10$	$-16 \le h \le 16$
	$-17 \le k \le 17$	$-31 \le k \le 31$	$-15 \le k \le 15$	$-19 \le k \le 18$
	$-17 \le l \le 18$	$-19 \le l \le 19$	$-21 \le l \le 21$	$-19 \le l \le 18$
Reflections collected	16 906	63 175	25 141	33 817
Data/restraints/parameters	8752/0/554	9000/0/541	7136/0/446	9618/0/550
Goodness-of-fit on F^2	1.031	1.023	1.058	1.084
Final R indexes [$I \ge 2\sigma(I)$]	R_1 = 0.0416	R_1 = 0.0350	R_1 = 0.0573	R_1 = 0.0318
	wR_2 = 0.1040	wR_2 = 0.0838	wR_2 = 0.1532	wR_2 = 0.0860
Final R indexes [all data]	R_1 = 0.0487	R_1 = 0.0485	R_1 = 0.0666	R_1 = 0.0337
	wR_2 = 0.1105	wR_2 = 0.0924	wR_2 = 0.1630	wR_2 = 0.0874
Largest diff. peak/hole (e Å^{-3})	0.64/−0.75	0.448/−0.339	1.983/−0.399	0.84/−0.62

multiple opportunities for hydrogen bonding as well as the fact that this water molecule is not involved in the synthons occurring in the anionic layers (*vide infra*). Compound **1** is identical to that reported during preparation of this manuscript[20] but we have included it here because a different description is provided and some theoretical studies on this compound are described below.

The 3-D architecture of this compound is shown in Fig. 2 and it exhibits several interesting features. The anionic $[Ni(hypydc)_2]^{2-}$ and cationic moieties form alternating 2-D layers (A and C, respectively). The cationic layer C is dominated by π···π interactions and the arrangement of the anionic layer is governed by H-bonding and π···π stacking interactions. It is worth mentioning that in both layers, stacking interactions are established between two anionic or two cationic moieties where a strong electrostatic repulsion is expected. Unexpectedly, the formation of stacking interactions between the protonated 9-aminoacridine aromatic ring and the chelidamic acid of the anionic complex are not observed, although a strong electrostatic attraction can be easily anticipated. The formation of stacking interactions between cationic aromatic rings has been previously described and studied in the literature,[33] especially in protonated aminopyridine moieties.[34] Obviously, the position of the counter-ion is crucial for stabilizing the $\pi^+\cdots\pi^+$ interaction. The A and C layers interact by means of strong electrostatic forces combined with N–H···O hydrogen bonding interactions (see Table 3) directly between counter-ions or through intervening water molecules.

The role of the water molecules stabilizing the anionic layer has been further analyzed. In Fig. 3 we show the anionic layer in more detail where the formation of $R_4^4(12)$ synthons involving two carboxylate groups and two symmetrically equivalent water molecules is highlighted. In addition, a $(H_2O)_4$ chain of water molecules is located between the $R_4^4(12)$ synthons and they are important for connecting the infinite 1-D chains of $[Ni(hypydc)_2]^{2-}$ anions to form the 2-D layer in conjunction with the $R_4^4(12)$ synthons.

3.3.2. Crystal structure of (H9a-Acr)$_2$[Co(hypydc)$_2$]·3H$_2$O (2). The asymmetric unit of **2** is shown in Fig. 4 together with the atomic numbering scheme while selected bond length and angles are summarized in Table 2. The anionic part is similar to that in **1** with the angle between the mean planes containing Co(1), O(1), C(1), C(2), N(1), C(6), C(7), O(2) and Co(1), O(6), C(8), C(9), N(2), C(13), C(14), O(7) is 83.47(2)°, close to that in **1**, but the *trans* N(1)–Co–N(2) angle is noticeably smaller (165.37(5)°). This aspect is further analyzed below *via* DFT studies. In the O_4N_2 environment the axial Co–N distances are 2.0125(14) and 2.0141(14) Å and the four equatorially coordinated atoms of the carboxylate groups (O(1), O(2), O(6), and O(7)) are at distances of 2.1597(12), 2.2315(12), 2.1467(12), and 2.1552(12) Å, respectively. The tetrahedral distortion of the equatorial substituents is indicated by the O(1)–Co(1)–O(2) and O(6)–Co(1)–O(7) angles of 151.95(4)° and 151.39(4)°, respectively. The asymmetric unit is completed by three water molecules and two protonated 9-aminoacridine molecules.

Table 2 Selected bond lengths (Å) and angles (°) for 1–4

1			
Ni1–O1	2.1449(14)	Ni1–N1	1.9685(16)
Ni1–O3	2.1188(15)	Ni1–N2	1.9636(15)
Ni1–O8	2.1419(14)	Ni1–O6	2.1226(14)
O1–C1	1.283(2)	O3–C7	1.274(2)
O2–C1	1.238(2)	N3–C27	1.361(3)
O3–Ni1–O1	154.79(5)	O3–Ni1–O6	88.17(6)
O3–Ni1–O8	96.35(6)	O6–Ni1 O1	96.06(6)
O6–Ni1–O8	155.36(5)	O8–Ni1–O1	90.10(5)
N1–Ni1–O1	77.10(6)	N1–Ni1–O3	77.80(6)
N1–Ni1–O6	105.02(6)	N1–Ni1–O8	99.61(6)
N2–Ni1–O1	107.58(6)	N2–Ni1–O3	97.61(6)
N1–Ni1–N2	174.48(7)		
2			
Co1–N1	2.0125(14)	Co1–O2	2.2315(12)
Co1–N2	2.0141(14)	Co1–O1	2.1597(12)
Co1–O6	2.1467(12)	Co1–O7	2.1552(12)
N1–Co1–N2	165.37(5)	N2–Co1–O1	118.54(5)
N1–Co1–O6	107.11(5)	N1–Co1–O1	75.88(5)
N2–Co1–O6	76.41(5)	O6–Co1–O7	151.39(4)
N1–Co1–O7	101.50(5)	N2–Co1–O7	75.89(5)
O6–Co1–O1	91.80(5)	O7–Co1–O2	86.65(5)
O7–Co1–O1	95.13(5)	O6–Co1–O2	99.96(5)
N1–Co1–O2	76.34(5)	N2–Co1–O2	89.09(5)
O1–Co1–O2	151.95(4)		
3			
Cr1–N2	1.967(2)	Cr1–O6	2.0051(17)
Cr1–N1	1.9727(19)	Cr1–O7	1.9989(17)
Cr1–O2	2.0001(18)	Cr1–O1	2.0118(18)
N2–Cr1–N1	175.49(8)	N1–Cr1–O1	78.13(8)
N2–Cr1–O2	97.19(8)	N2–Cr1–O1	106.24(8)
N1–Cr1–O2	78.45(7)	N2–Cr1–O7	78.23(7)
N1–Cr1–O7	100.63(7)	O7–Cr1–O6	156.80(7)
O2–Cr1–O7	9193(8)	N2–Cr1–O6	78.59(8)
N1–Cr1–O6	102.55(7)	O2–Cr1–O6	91.82(7)
O1–Cr1–O2	156.58(7)		
4			
Cd1–O1	2.3278(14)	N3–C27	1.364(2)
Cd1–O3	2.3496(14)	N4–C21	1.325(2)
Cd1–O6	2.3562(13)	C15–C16	1.415(3)
Cd1–O8	2.3378(14)	C15–C20	1.414(2)
Cd1–N1	2.2111(16)	C16–C17	1.371(3)
Cd1–N2	2.1889(16)	C17–C18	1.412(3)
O1–Cd1–O3	141.74(5)	N2–C13–C14	114.89(16)
O1–Cd1–O6	87.60(5)	C12–C13–C14	123.05(16)
O1–Cd1–O8	105.53(5)	O8–C14–C13	116.14(16)
O3–Cd1–O6	104.93(5)	O9–C14–O8	126.32(17)
O8–Cd1–O3	86.14(5)	O9–C14–C13	117.54(17)
O8–Cd1–O6	142.96(5)	C15–N3–C27	122.05(16)
N1–Cd1–O1	71.26(5)	N3–C15–C16	118.62(16)
N1–Cd1–O3	70.55(5)	N3–C15–C20	120.88(17)
N1–Cd1–O6	105.85(5)	C20–C15–C16	120.49(17)
N1–Cd1–O8	111.15(5)	C17–C16–C15	119.34(18)

Although one might predict **1** and **2** to have very similar structures, this is not the case as they crystallize in different space groups and with different numbers of water molecules. Nevertheless, the 3-D architecture of this compound exhibits some similarities with **1**. Thus, the solid state structure is also arranged in alternating anionic and cationic 2-D layers (A and C, respectively). The cationic layer C is dominated by two types of π···π interactions that for this particular compound are characterized by simultaneous parallel and antiparallel binding modes (see Fig. 5). The π···π stacking interaction in the anionic part is almost identical to the observed for **1**, where two strong hydrogen bonds involving the phenolic carboxylate groups are established. The A and C layers interact by means of strong electrostatic forces combined with O–H···O and N–H···O hydrogen bonding interactions (see Table 3) directly between counter-ions or through intervening water molecules as observed for **1**.

A closer view of the anionic layer is shown in Fig. 6. The combination of π···π and hydrogen bonding interactions (see Fig. 5, bottom-right) is responsible for the formation of infinite 1-D chains, since each chelidamic acid ligand of the anionic moiety $[Co(hypydc)_2]^{2-}$ establishes a π···π stacking interaction prolonging the chain. The 2-D layer is generated by means of bridging water molecules creating $R_6^6(20)$ synthons (see Fig. 6). The π···π and H-bonding interactions that create the infinite 1-D chain are also highlighted in Fig. 6.

3.3.3 Crystal structure of (H9a-Acr)[Cr(hypydc)$_2$]·4H$_2$O (3). The asymmetric unit of **3** is shown in Fig. 7 together with the atomic numbering scheme while Table 2 summarizes selected bond length and angles. In the $[Cr(hypydc)_2]^{2-}$ anion, we find the shortest metal–ligand distances of the series as expected due to the smaller Cr(III) ion. The axial Cr–N distances are 1.967(2) and 1.9727(19) Å and the *trans* N(1)–Cr–N(2) angle is 175.49(8)° while the angle between the mean planes containing Cr(1), O(1), C(1), C(2), N(1), C(6), C(7), O(2) and Co(1), O(6), C(8), C(9), N(2), C(13), C(14), O(7) is 89.06(4)°. The four equatorially coordinated atoms are O(1), O(2), O(6), and O(7) of the carboxylate groups at distances of 2.0118(18), 2.0001(18), 2.0051(17), and 1.9989(17) Å, respectively, and showing a tetrahedral distortion as indicated by O(1)–Cr(1)–O(2) and O(6)–Cr(1)–O(7) angles of 156.58(7)° and 156.80(7)°, respectively. The asymmetric unit is completed by 3.5 water molecules (*i.e.* 7 molecules per unit cell), one of which is disordered over two sites in a 0.70/0.30 (O(12)) ratio while the remainder, with the exception of O(11), show partial site occupancy as well as disorder over two sites and two half molecules of 9-aminoacridine, each of which is protonated at the ring nitrogen and disordered across a centre of symmetry. Because of this disorder, not all hydrogen atoms of the water molecules could be located with confidence so the full hydrogen bonding network could not be determined. In general, there are a number of voids of varying size and potential for hydrogen bonding between the cations and anions in **1** and **3** which can be filled with lattice water molecules. It is thus not surprising that we observe incomplete occupancy in some of these sites as is the case for **1** and **3**. In the latter structure, this is complicated by the disorder observed for the cations. Here the elongated displacement ellipsoids seen for O12 and O15 likely indicate unresolved additional disorder for these atoms.

Table 3 Hydrogen bond parameters (distances in Å, and angles in °) for 1–4[a] [30]

D–H···A	d(D–H)/Å	D(H–A)/Å	d(D–A)/Å	D–H–A/°
Compound 1				
O(5)–H(5O)···O(8)[1]	0.84	1.74	2.576(2)	171
O(10)–H(10O)···O(1)[2]	0.84	1.76	2.589(2)	170
N(3)–H(3N)···O(7)[3]	0.91	1.92	2.824(2)	173
N(4)–H(4A)···O(14)[4]	0.88	1.84	2.675(4)	157
N(4)–H(4B)···O(9)[5]	0.88	2.03	2.904(3)	174
N(5)–H(5N)···O(13)	0.91	1.9	2.809(2)	173
N(6)–H(6A)···O(6)[3]	0.88	2	2.863(2)	168
N(6)–H(6B)···O(11)[6]	0.88	1.94	2.812(2)	173
O(11)–H(11A)···O(4)[7]	0.84	2.04	2.839(2)	157
O(11)–H(11B)···O(3)	0.84	1.91	2.744(2)	172
O(12)–H(12A)···O(2)[2]	0.84	1.99	2.823(2)	174
O(12)–H(12B)···O(14)[8]	0.84	2.15	2.964(4)	163
O(13)–H(13A)···O(12)	0.85	2.36	2.834(2)	115
O(13)–H(13B)···O(4)[7]	0.84	2.02	2.857(2)	174
O(14)–H(14A)···O(7)[3]	0.84	1.99	2.773(4)	155
O(14)–H(14B)···O(12)[3]	0.84	2.13	2.964(4)	173
Compound 2				
O(5)–H(5O)···O(7)[4]	0.84	1.72	2.5366(17)	163
O(10)–H(10O)···O(2)[9]	0.84	1.81	2.6241(17)	161
N(3)–H(3N)···O(11)[10]	0.91	1.84	2.7537(19)	179
N(4)–H(4B)···O(1)[11]	0.91	2.02	2.9024(18)	162
N(5)–H(5N)···O(8)[12]	0.91	1.94	2.8172(18)	161
N(6)–H(6A)···O(3)[6]	0.91	1.97	2.8030(18)	151
N(6)–H(6B)···O(13)[11]	0.91	2.01	2.8844(19)	161
O(11)–H(11A)···O(6)[11]	0.84	2	2.8242(17)	167
O(11)–H(11B)···O(12)[13]	0.84	2	2.8024(18)	160
O(12)–H(12A)···O(3)	0.84	1.94	2.7728(18)	175
O(12)–H(12B)···O(4)[11]	0.84	2.14	2.9098(17)	152
O(13)–H(13A)···O(9)	0.84	2	2.8165(18)	166
O(13)–H(13B)···O(12)[11]	0.84	2.04	2.8638(19)	166
Compound 3				
O(5)–H(5O)···O(11)	0.84	1.78	2.615(3)	173
O(10)–H(10O)···O(12)[14]	0.84	1.7	2.527(3)	166
O(10)–H(10O)···O(12A)[14]	0.84	1.8	2.623(3)	166
N(3)–H(3A)···O(7)[8]	0.91	2.28	3.143(5)	158
N(3)–H(3B)···O(13)[11]	0.91	2.38	3.233(6)	166
N(4)–H(4N)···O(14)	0.91	1.78	2.671(5)	165
N(5)–H(5A)···O(8)[5]	0.91	2.04	2.937(5)	167
N(6)–H(6N)···O(15)	0.91	1.7	2.601(10)	171
N(6)–H(6N)···O(15A)	0.91	1.64	2.487(13)	153
O(11)–H(11A)···O(6)[11]	0.84	1.92	2.739(3)	166
O(11)–H(11B)···O(3)[15]	0.84	2.12	2.953(3)	174
O(12)–H(12A)···O(9)[15]	0.84	1.96	2.744(4)	156
O(12)–H(12B)···O(2)[11]	0.84	2.02	2.813(3)	157
O(13)–H(13A)···O(3)[11]	0.84	2.23	2.841(4)	179
O(13)–H(13B)···O(4)[10]	0.84	2.23	2.974(4)	147
O(13A)–H(13C)···O(5)	0.84	2.07	2.63(4)	124
O(14)–H(14A)···O(13)[11]	0.84	1.73	2.563(7)	170
O(15)–H(15A)···O(13)	0.84	2.04	2.657(10)	130
Compound 4				
O(5)–H(5O)···O(6)[17]	0.84	1.76	2.587(2)	169
O(10)–H(10O)···O[16]	0.84	1.75	2.565(2)	162
N(3)–H(3N)···O9	0.91	1.91	2.812(2)	169
N(4)–H(4A)···O(12)[5]	0.91	2.32	3.224(3)	172
N(4)–H(4B)···O(7)[5]	0.91	2.04	2.935(2)	165
N(5)–H(5N)···O(13)[11]	0.91	1.92	2.802(2)	163
N(6)–H(6A)···O(8)	0.91	2.04	2.924(2)	163
N(6)–H(6B)···O(11)[6]	0.91	1.91	2.799(2)	165
O(11)–H(11A)···O(4)[6]	0.84	2.03	2.825(2)	157
O(11)–H(11B)···O(3)[8]	0.84	1.9	2.7360(19)	170
O(12)–H(12A)···O(14)[8]	0.84	2.24	3.028(2)	156

Table 3 *(continued)*

Compound 4				
O(12)–H(12B)···O(9)^{11}	0.84	2.36	2.988(2)	132
O(13)–H(13A)···O(14)	0.84	2.01	2.840(2)	172
O(13)–H(13B)···O(4)^{13}	0.84	1.99	2.823(2)	172
O(14)–H(14A)···O(2)	0.84	1.98	2.817(2)	177
O(14)–H(14B)···O(12)^{9}	0.84	2.07	2.890(3)	166

[a] Symmetry codes: (1) 2 − *x*, −*y*, 2 − *z*; (2) 1 − *x*. −*y*, 1 − *z*; (3) *x*, 1 + *y*, *z*; (4) 1 − *x*, 1 − *y*, 1 − *z*; (5) *x*, *y*, *z* − 1; (6) 2 − *x*, 1 − *y*, 1 − *z*; (7) *x*, *y* − 1, *z*; (8) *x*, *y* − 1, *z*; (9) 1 − *x*, 1 − *y*, 2 − *z*; (10) −*x*, 1/2 + *y*, 1/2 − *z*; (11) 1 − *x*, 1 − *y*, 1 − *z*; (12) *x*, 1.5 + *y*, *z* − 1/2; (13) *x* − 1, *y*, *z*; (14) *x*, 1 + *y*, *z* − 1; (15) −*x*, 1 − *y*, 1 − *z*; (16) 1 − *x*, 2 − *y*, 1 − *z*; (17) 2 − *x*, 2 − *y*, 2 − *z*.

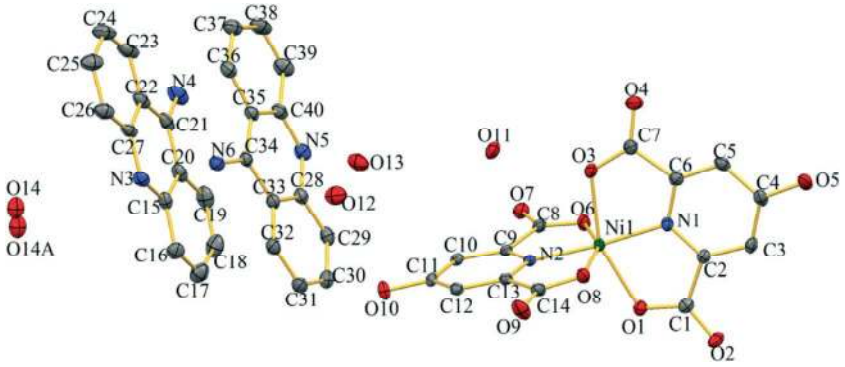

Fig. 1 Perspective view of **1** showing the atom labeling scheme. Ellipsoids are drawn at the 50% probability level and hydrogen atoms are omitted for clarity. Both components of the disorder for O14 are shown.

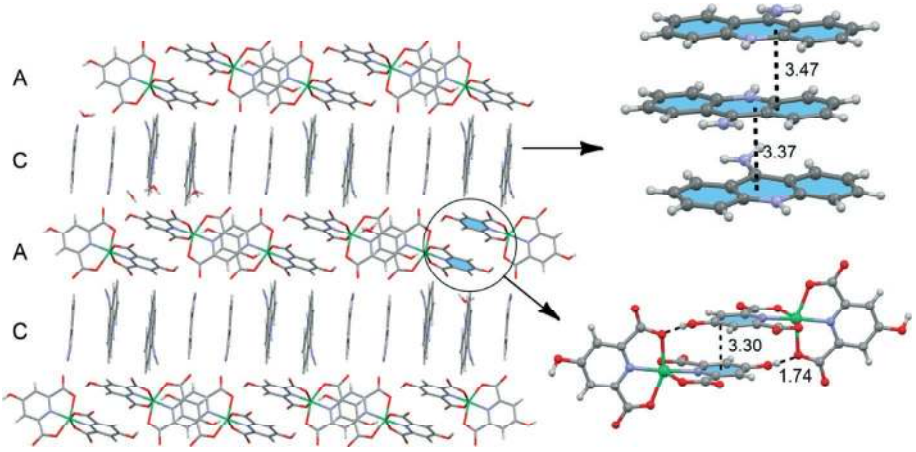

Fig. 2 3-D packing of **1** showing alternating anionic (A) and cationic (C) layers. The stacking interactions observed in both layers are highlighted at the right side of the figure. Distances in Å.

The 3-D architecture of this compound is shown in Fig. 8 and it is completely different from that observed for **1** and **2**. In this case the formation of anionic/cationic layers is not observed but rather a grid-like arrangement is produced (see Fig. 8). This is due to the formation of very strong $\pi^{+}\cdots\pi^{-}$ contacts that combine strong electrostatic forces with aromatic stacking interactions. The grid is formed due to the perpendicular disposition of the chelidamic acids in the anionic part that generates a perpendicular arrangement of the counter-ions upon formation of the stacking complexes and, consequently, the final 3-D architecture is completely different from that observed for **1** and **2**, where isolated $\pi^{+}\cdots\pi^{-}$ and $\pi^{-}\cdots\pi^{-}$ stacking interactions were formed. One reason for the different 3-D architecture for **3** is its stoichiometry which has a cation/anion ratio of 1 : 1 instead of the 2 : 1 ratio for **1**, **2** and **4**. In the latter three compounds, the asymmetric unit contains two independent cations so there is no crystallographic restriction on their locations with respect to one another in the unit cell. In the former, however, there is only one and it can only occupy positions

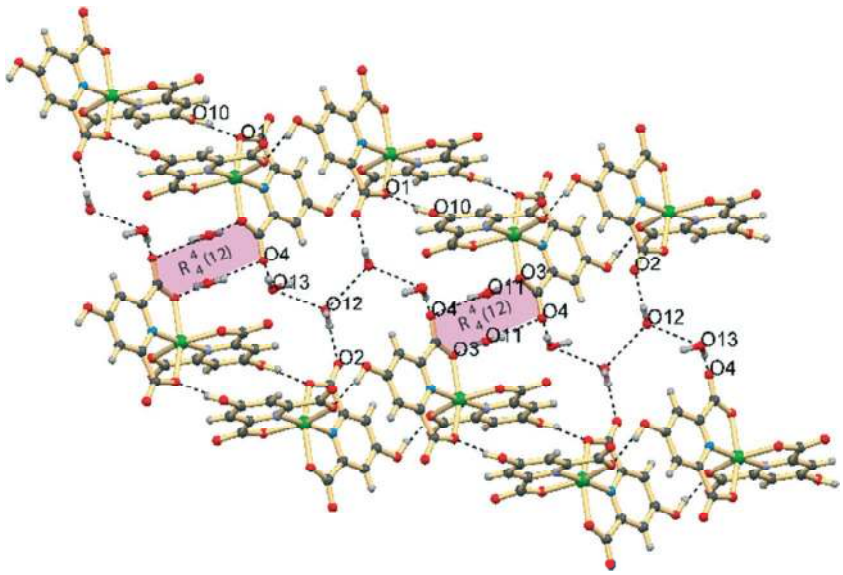

Fig. 3 View of the anionic part in **1** along the *b* axis showing $R_4^4(12)$ synthons and $(H_2O)_4$ chains.

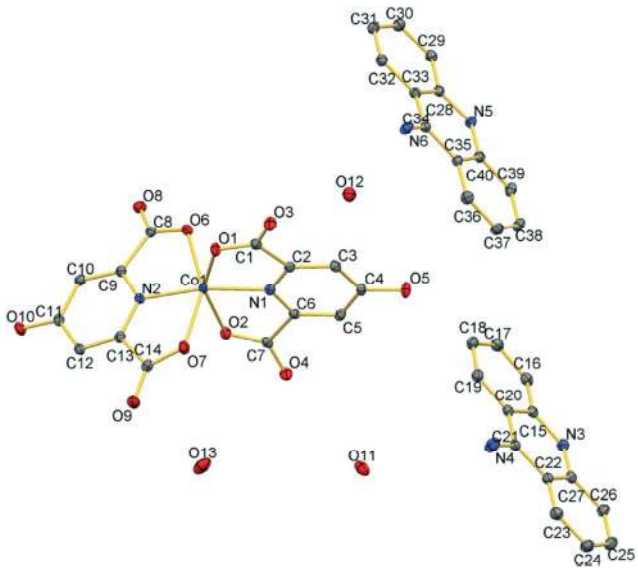

Fig. 4 Perspective view of **2** showing the atom labeling scheme. Ellipsoids are drawn at the 50% probability level and hydrogen atoms are omitted for clarity.

dictated by the symmetry operations of the space group. Thus in **3**, the cations are not able to associate closely as is the case in the other structures. It is worth mentioning the crucial role of aromatic interactions on the final architectures of these complexes even in the presence of strong hydrogen bonding interactions.

3.3.4 Crystal structure of $(H9a\text{-}Acr)_2[Cd(hypydc)_2]\cdot 4H_2O$ (4). The asymmetric unit of **4** is shown in Fig. 9 together with the atomic numbering scheme and selected bond lengths and angles are summarized in Table 2. The distorted octahedral N_2O_4 environment of the metal can be characterized by axial Cd–N distances of 2.2111(16) and 2.1889(16) Å, a *trans* N(1)–Cd(1)–N(2) angle of 171.42(5)° and an angle between the mean planes Cd(1), O(1), N(1), O(3) and Cd(1), O(6), N(2), O(8) of 80.34(5)°. The four equatorially coordinated atoms are O(1), O(3), O(6), and O(8) of the carboxylate groups at distances of 2.3278(14), 2.3496(14), 2.3562(13), 2.3378(14) Å, respectively with a significantly greater tetrahedral distortion than in **1**–**3** indicated by the O(1)–Cd(1)–O(3) and O(6)–Cd(1)–O(8) angles of 141.74(5)° and 142.96(5)°, respectively. The asymmetric unit is completed by four water molecules and two protonated 9-aminoacridine molecules that are arranged similarly to that observed in complex **1**.

The 3-D architecture of **4** is shown in Fig. 10 and it exhibits several interesting features. Similarly to **1** and **2** and by contrast to **3**, the anionic $[Cd(hypydc)_2]^{2-}$ and cationic moieties form alternating 2-D layers (A and C, respectively). The cationic layer C is dominated by π···π interactions and the arrangement of the anionic layer is governed by H-bonding and π···π stacking interactions. The A and C layers interact by means of strong electrostatic forces complemented by N–H···O hydrogen bonding interactions (see Table 3) directly between counter-ions or through intervening water molecules. The π···π interactions of the cationic layers are similar to that found in compound **1** where the arrangement of the 9-aminoacridine molecules is a combination of an almost perfect antiparallel stacking with a mostly antiparallel arrangement where one molecule is rotated (~28°) with respect to the other two (see Fig. 10, top-right). The π···π stacking distance of the anionic part is longer than the rest of the compounds probably due to the longer Cd–O distances observed in **4** with respect to the rest of the $[M(hypydc)_2]^{2-}$ complexes.

As also observed in **1** and **2**, the role of the water molecules is crucial for stabilizing the anionic layer. In Fig. 11 we have represented the anionic layer in more detail

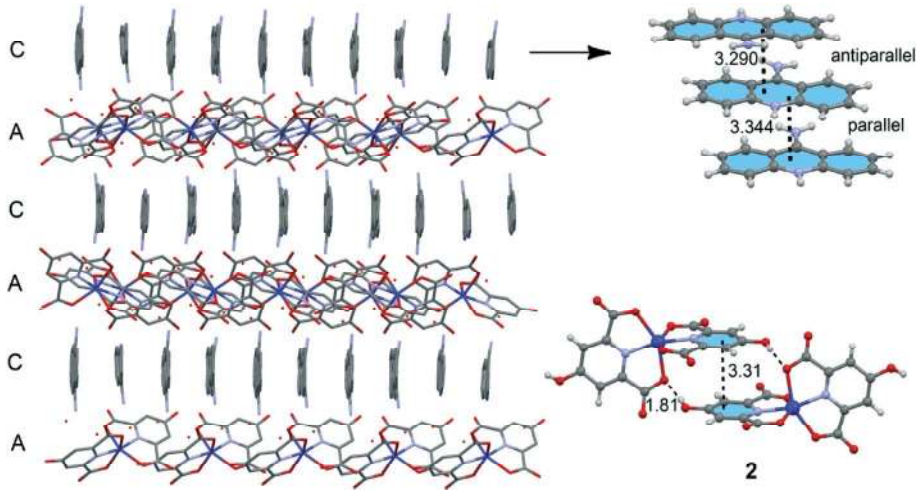

Fig. 5 3-D packing of **2** showing alternating anionic (A) and cationic (C) layers. The stacking interactions observed in both layers are highlighted at the right side of the figure. Distances in Å are measured from the mean plane of one molecule to the closest ring atom of the other.

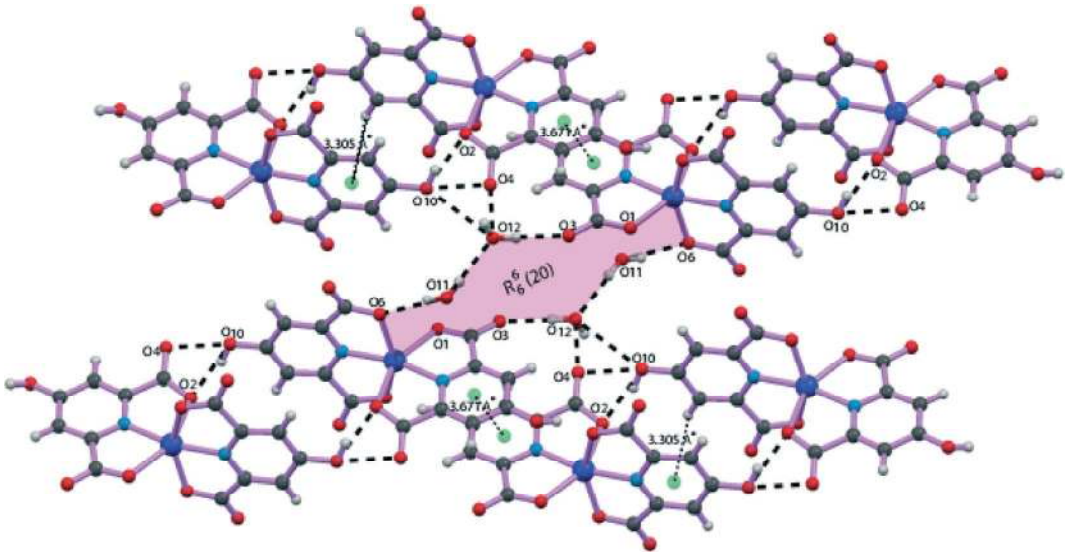

Fig. 6 View of the anionic portion of **2** along the *b* axis showing π···π interactions and the O–H···O hydrogen bonds making $R_6^6(20)$ synthons.

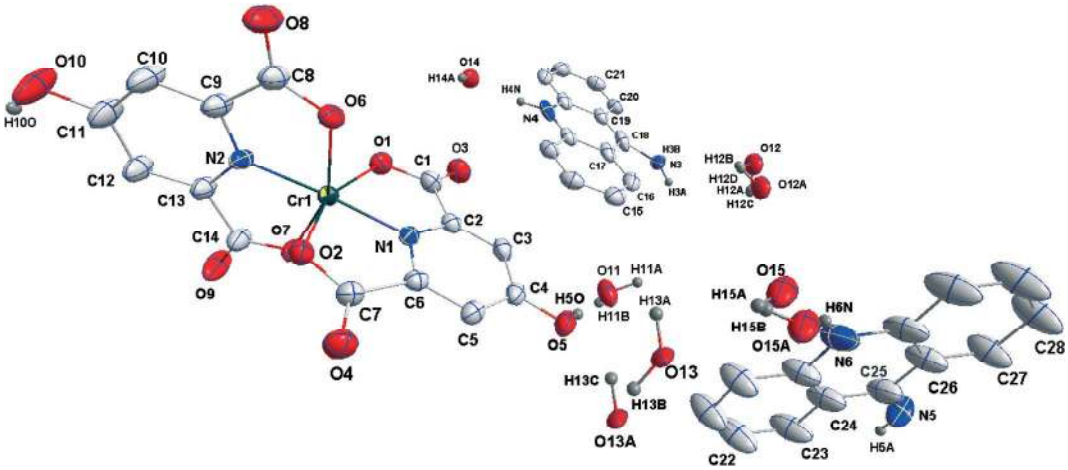

Fig. 7 Perspective view of **3** showing the atom labeling scheme. Ellipsoids are drawn at the 50% probability level and H-atoms attached to carbon are omitted for clarity.

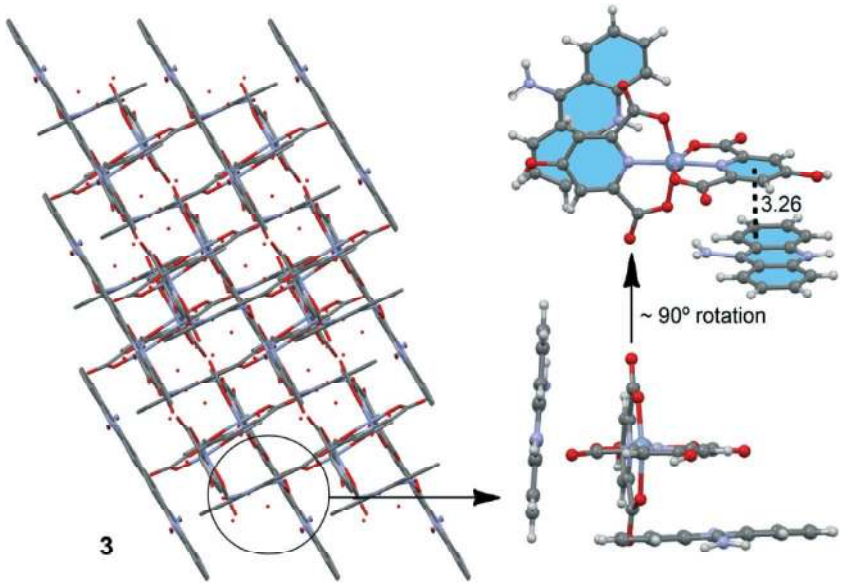

Fig. 8 3-D packing of **3** showing the grid structure. The stacking interactions between counter-ions are highlighted at the right side of the figure. Distances in Å are measured from the mean plane of one molecule to the closest ring atom of the other.

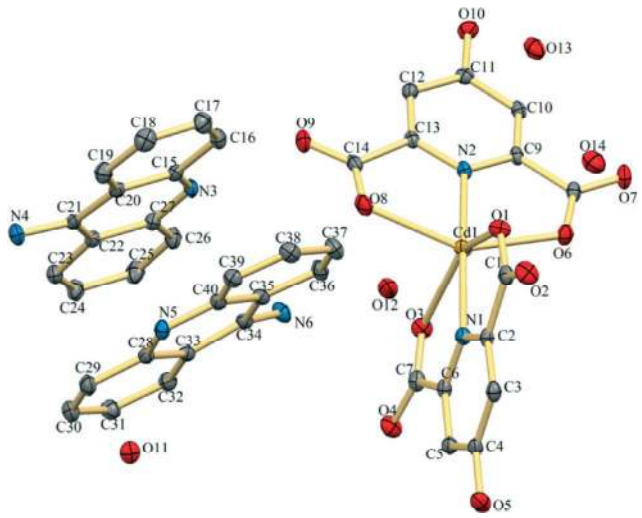

Fig. 9 Perspective view of **4** showing the atom labeling scheme. Ellipsoids are drawn at the 50% probability level and hydrogen atoms are omitted for clarity.

to show the formation of $R_4^4(12)$ synthons involving two carboxylate groups and two symmetrically equivalent water molecules. In addition, a $(H_2O)_4$ cluster of water molecules is located between the $R_4^4(12)$ synthons connecting the infinite 1-D chains of $[Cd(hypydc)_2]^{2-}$ anions to form the 2-D layer in conjunction with the $R_4^4(12)$ synthons.

The structural results for **1–4** can be compared with those of other salts of $[M(hypydc)_2]^{n-}$ anions. In $[C_3H_7N_3]_2[Cu(hypydc)_2]$,[12] $[C_5H_8N_3][Cr(hypydc)_2]$,[35] $[C_5H_8N_3][Fe(hypydc)_2]\cdot 2H_2O$,[36] $[C_{13}H_{10}N_2]_2[Zn(hypydc)_2]\cdot 10H_2O$,[37] $[C_{13}H_{10}N_2][Fe(hypydc)_2]\cdot 4.5H_2O$[37] and $[C_4H_{12}N_2]_{0.5}[Ga(hypydc)_2]\cdot H_2hypydc\cdot 2H_2O$[38] the *trans* N–M–N and *trans* O–M–O angles are similar to those reported herein except for the gallium complex, where the reported N–Ga–N angle is 171.11(7)°. By contrast in the $[C_3H_{12}N_2][Zn(hypydc)_2]\cdot 3.5H_2O$ complex,[39] the N–Zn–N angle is 157.0(1)° while the *trans* O–Zn–O angles are similar to those observed in our complexes. In the latter study, the authors do not comment on the significant non-linearity of the N–Zn–N angle of the coordination sphere, which is likely due to the large number of intermolecular contacts formed by the ligands in the solid state, as we observed in **2**.

3.4. DFT calculations.

We have performed a computational study in order to further analyze the significantly smaller *trans* N–M–N angle observed in **2** (165°), as compared to the rest of complexes (>172°). We have studied how the relative formation energy of the $[M(hypydc)_2]^{2-}$ moiety changes as the *trans* N–M–N angle varies from 180° to 150° to assess the energetic cost of the bending. The optimized geometries of compounds **1–4** are shown in Fig. 12. It can be observed that the optimized value for the *trans* angle is in all cases close to linearity. Therefore the smaller angle observed in the solid state of **2** is due to additional forces that stabilize that conformation.

Inspection of the results shown in Fig. 13 leads to some interesting conclusions. First, the most favorable conformation in all cases is found at a *trans* N–M–N angle close to 180° and a different behavior of the complexes is observed at values smaller than 175. It is clear that the relative energies of **1**(Ni) and **3**(Cr) are more affected by the variation of the angle. This behavior is likely related to the crystal field stabilization energy (CFSE). Obviously the Cd complex has 0 CFSE and it is the complex with the smallest energetic cost for the bending while the CFSE for high-spin Co(II) is $0.8\Delta_o$.

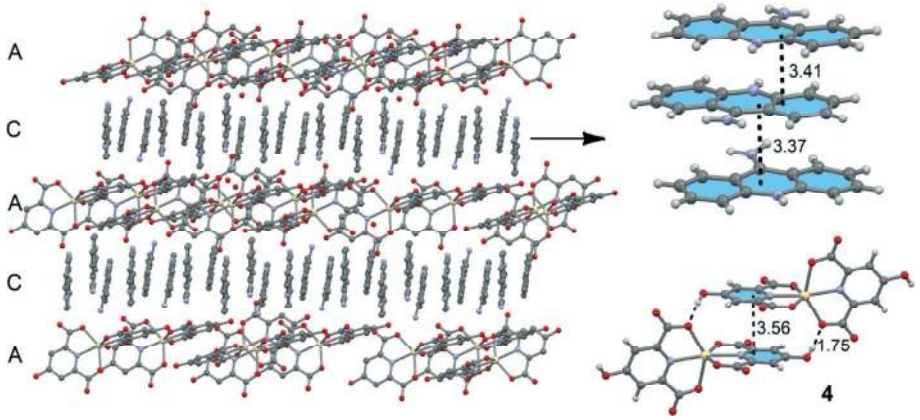

Fig. 10 3-D packing of **4** showing alternating anionic (A) and cationic (C) layers. The stacking interactions observed in both layers are highlighted at the right side of the figure. Distances in Å are measured from the mean plane of one molecule to the closest ring atom of the other.

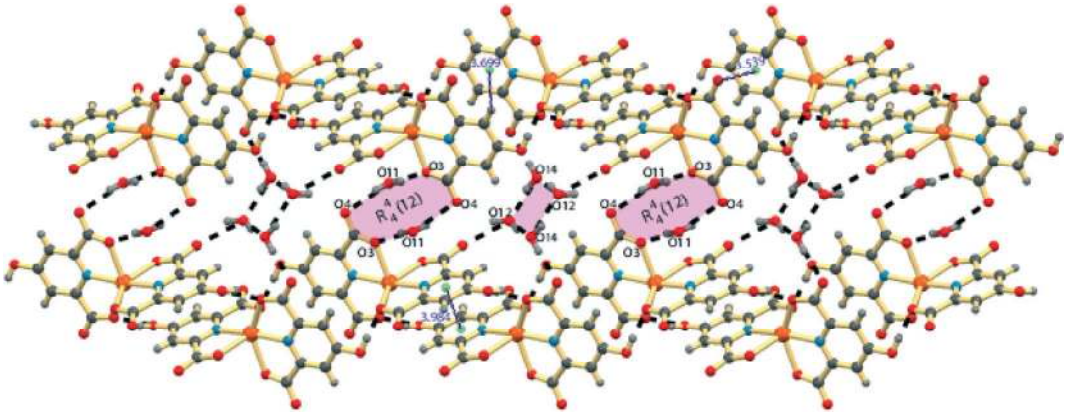

Fig. 11 Presentation of the anionic portion of **4** along the *b* axis showing the $R_4^4(12)$ synthons and the square water clusters.

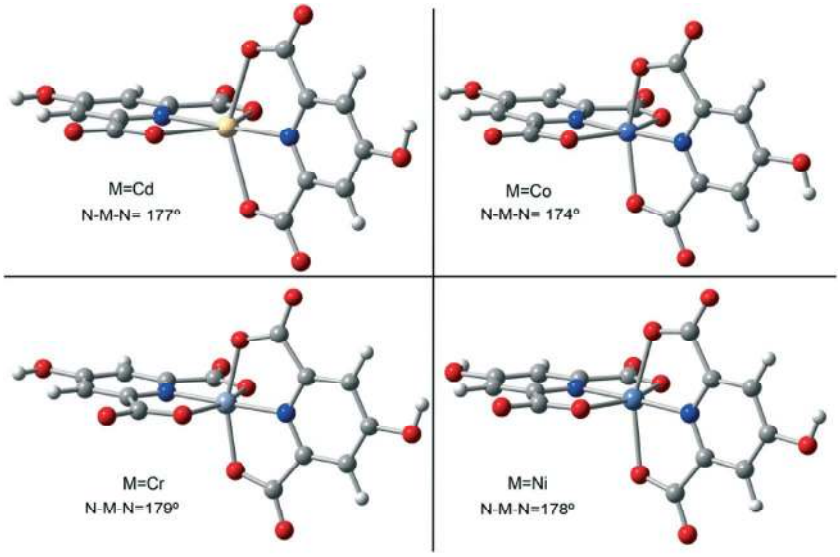

Fig. 12 Optimized geometries of compounds **1**–**4**.

By contrast, the CFSE for Ni(II) and Cr(III) is $1.2\Delta_o$ with the actual value for Cr(III) being larger than for Ni(II) because of the larger Δ_o for the former. The energetic results shown in Fig. 13 are consistent with the expected trend in CSFE for the four complexes. Thus, at 150°, compounds **1** and **3** are more destabilized than the other two. Interestingly, at 165°

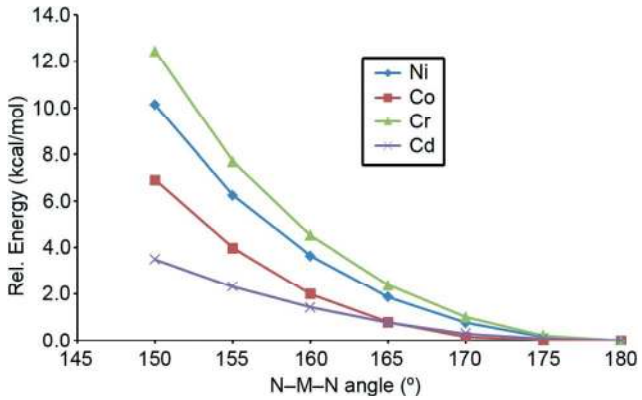

Fig. 13 Comparison of the relative energies of complexes **1**–**4** at different *trans* N–M–N angles.

complexes 2(Co) and 4(Cd) have the same relative energy that is very small (0.8 kcal mol^{-1}). Therefore for these complexes the energetic cost of bending the N–M–N (M = Co, Cd) angle from 180° to 165° is almost negligible. Consequently, any additional force present in the solid state can easily influence the final N–Co–N angle, as it occurs in 2. We have also studied theoretically the $\pi^{-}\cdots\pi^{-}$ stacked interactions that play a critical role in the final solid state architecture of compounds **1**, **2**, and **4**. Firstly, we have studied the $\pi^{-}\cdots\pi^{-}$ stacking interaction in complex **1**. The theoretical model used to compute the $\pi^{-}\cdots\pi^{-}$ interaction is shown in Fig. 14, where the 9-aminoacridine fragments (counter-ions) have been simplified in order to keep the system computationally tractable. Without the consideration of the counter-ions the interaction is obviously unfavorable due to a strong electrostatic repulsion. The binding energy using the model of Fig. 14 where the counter-ions have been considered is −37.3 kcal mol^{-1}, which is very large and negative due to the neutral nature of the complete system. As can be observed in the model, the $\pi^{-}\cdots\pi^{-}$ stacking interaction is accompanied by two hydrogen bonds formed between the chelidamic acid moieties. This binding mode, where $\pi^{-}\cdots\pi^{-}$ stacking and hydrogen bonds work in concert, is observed in compounds **1**, **2**, and **4** and it is responsible for the deviation from linearity of the N–M–N angle. The different degree of deviation is modulated by the different cost of bending this angle.

Moreover, we have studied the $\pi^{-}\cdots\pi^{-}$ interaction observed in **3**, formed by one $[Cr(hypydc)_2]^{2-}$ moiety unit and two amino-anthracene counter-ions. The theoretical model used is shown in Fig. 15. Since this $\pi^{+}\cdots\pi^{-}$ stacking has a critical impact on the final solid state architecture, we have evaluated its strength resulting in a binding energy value of −167.9 kcal mol^{-1}. This result is very large and negative, due to the strong electrostatic component of the $\pi^{+}\cdots\pi^{-}$ complex.

An important aspect of this study is the different solid state structure of compound **3** where the cation/anion ratio is 1 : 1 compared to that adopted by the other compounds (**1**, **2** and **4**) where it is 2 : 1 and we have noted above the restriction that this places on the locations of the cations in **3** which is absent for the others. To this respect the different types of stacking interactions ($\pi^{+}\cdots\pi^{-}$, $\pi^{-}\cdots\pi^{-}$ and $\pi^{-}\cdots\pi^{-}$) observed in compounds **1**–**4** are certainly important. It is worth mentioning that the $\pi^{+}\cdots\pi^{-}$ interaction exhibit a very strong binding energy, though this motif is only observed in one compound (**3**). A likely explanation is that the electrostatic interaction between the 2D anionic and cationic layers compensates the strong $\pi^{+}\cdots\pi^{-}$ interaction in the other complexes. We have further analyzed this aspect theoretically by performing additional calculations. After a careful examination of the interaction between layers, we have found three different binding motifs between the anionic $[M(hypydc)_2]^{2-}$ moiety and protonated 9-aminoacridine fragments (counter-ions). They are represented in Fig. 16 together with their associated interaction energies, using compound **4** as a model. One of both $\pi^{+}\cdots\pi^{-}$ interactions (see Fig. 8) observed in compound **3** has been evaluated before (−167.9 kcal mol^{-1}, see Fig. 15), and the interaction energy of the other $\pi^{-}\cdots\pi^{-}$ interaction is very similar (−168.7 kcal mol^{-1}), therefore the total stabilization energy is −336.6 kcal mol^{-1}. In compound **4**, the sum of the three interactions observed for the anionic

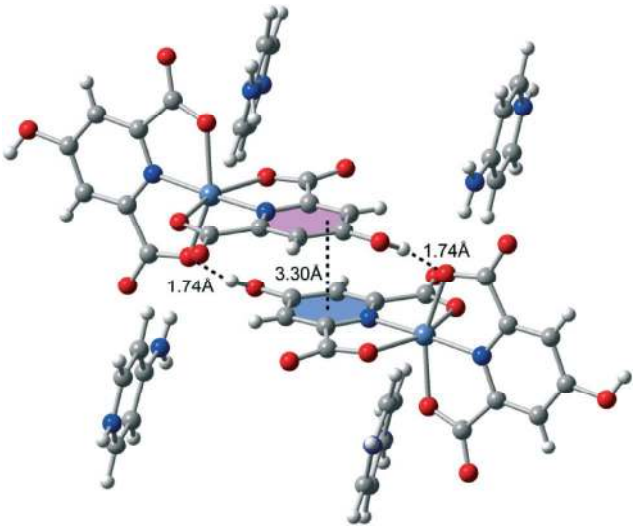

Fig. 14 Theoretical model used to compute the stacking interaction present in **1**.

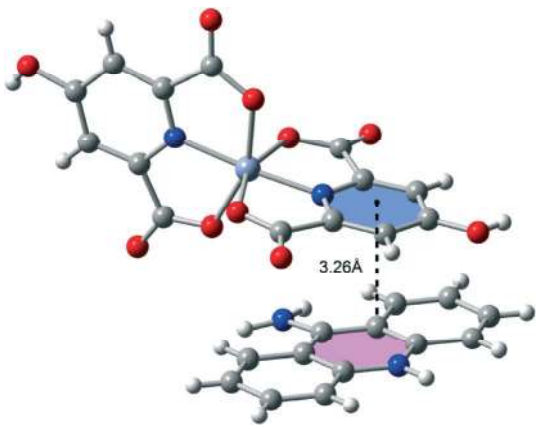

Fig. 15 Theoretical model used to evaluate the $\pi^{+}\cdots\pi^{-}$ interaction.

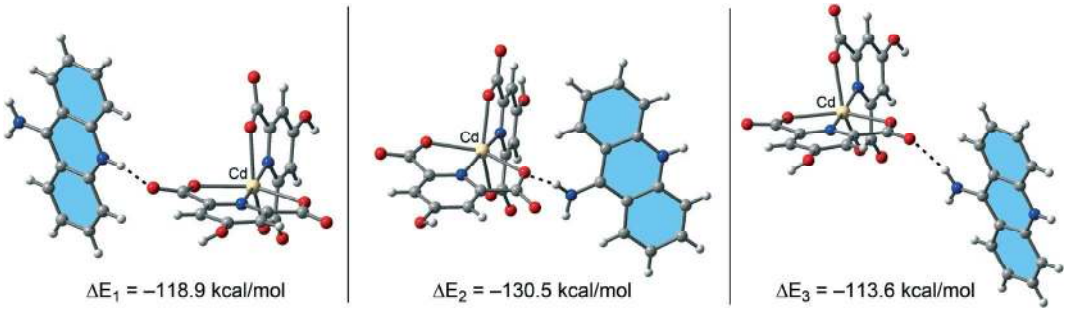

Fig. 16 Three interaction modes observed in compound **4** that are responsible for the assembly of 2D cationic and anionic layers in the solid state and their interaction energies.

moiety interacting with the protonated 9-aminoacridine is more favorable ($\Delta E_1 + \Delta E_2 + \Delta E_3 = -362.9$ kcal mol^{-1}). The existence of many other factors in the solid state like the presence of water molecules or differences in the coordination ability of the metal center may influence the formation of either the cationic/anionic 2D layers observed in **1**, **2** and **4** or a 3D grid structure governed by $\pi^{-}\cdots\pi^{-}$ interactions observed in **3** that is energetically less favorable.

3.5. Solution studies

In preliminary experiments, the fully protonated forms of H_2hypydc (L) and 9a-Acr (Q), as the building blocks of the self-associated system and their 1 : 1 mixture were titrated in a 50% methanol–50% water mixture in the absence and presence of the metal ions with a 0.059 M solution of LiOH at a temperature of 25 °C and an ionic strength of 0.1 M, maintained by $NaNO_3$. The resulting titration curves for L and Q are shown in Fig. 17(a) and (b). The pH titration data in the absence of metal ions were used to calculate the protonation constants for L and Q (K_n^{H} $[H_nL]/[H_{(n-n)}L][H]^n$, the charges are omitted for simplicity) *via* the program BEST.[31] The resulting values for the overall stability and stepwise protonation constants of L and Q as well as the recognition constants for the L–Q proton transfer system are listed in Table 4.

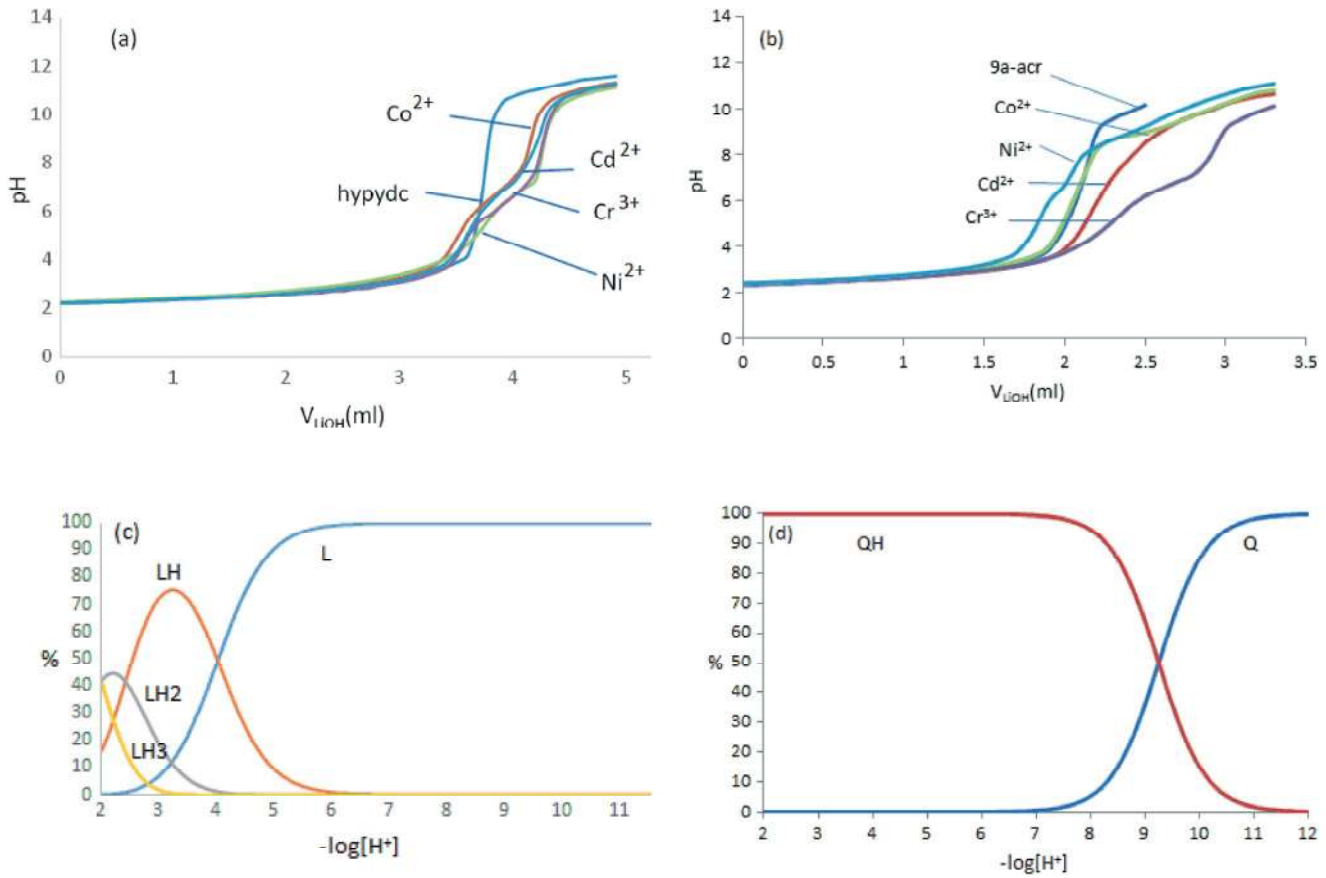

Fig. 17 Potentiometric titration curves of hypydc (a) and 9a-Acr (b) in the absence and presence of Co^{2+}, Ni^{2+}, Cd^{2+}, and Cr^{3+} ions with LiOH 0.059 M in a 50% methanol–50% water solvent at 25 °C and μ = 0.1 M $NaNO_3$, and distribution diagrams of hypydc (L) (c) and 9a-Acr (Q) (d).

Table 4 Overall stability and stepwise protonation constants of H_2hypydc and 9a-Acr and their recognition constants for in a 50% methanol–50% water at 25 °C and μ = 0.1 M $NaNO_3$

Stoichiometry							
H_2hypydc	9a-Acr	h	log β	Equilibrium quotient K	log K	Max%	pH
1	0	1	4.1	—	4.1	75.3	3.2
1	0	2	6.54	—	2.44	44.6	2.2
1	0	3	9.09	—	2.55	41.4	2
0	1	1	9.25	—	9.25	99.9	2–6.2
1	1	1	15.28	[9a-AcrHhypydc]/[H9a-Acr][hypydc]	6.03	25.4	4.4
1	1	2	18.53	[9a-AcrH_2hypydc]/[H9a-Acr][Hhypydc]	5.18	36.6	2
2	2	0	17.29	$[(9a\text{-}Acr)_2(hypydc)_2]/[9a\text{-}Acr]_2[hypydc]_2$	—	62.2	10.2
2	2	1	27.12	$[(H9a\text{-}Acr)(9a\text{-}Acr)(hypydc)_2]/[9a\text{-}Acr][H9a\text{-}Acr][hypydc]_2$	17.87	99.4	7.1–7.6
2	2	3	36.01	$[(9a\text{-}AcrH)_2(Hhypydc)(hypydc)]/[9a\text{-}AcrH]_2[Hhypydc][hypydc]$	8.26	90.4	3
2	2	−1	5.92	$[(9a\text{-}Acr)_2(hypydc)_2(OH)]/[9a\text{-}Acr]_2[hypydc]_2[OH]$	—	4.3	10.7
2	2	−2	−4.05	$[(9a\text{-}Acr)_2(hypydc)_2(OH)_2]/[9a\text{-}Acr]_2[hypydc]_2[OH]_2$	—	49.2	11.9

The corresponding species distribution diagrams for L, Q, and their mixtures are shown in Fig. 17(c), (d) and 18, respectively. As it is obvious from Table 4 and the corresponding distribution diagrams, the most likely proton transfer species between L and Q with a 2:2 stoichiometry are: L_2Q_2H (99.4% at pH 7.1–7.6 with log K 17.87) and $L_2Q_2H_3$ (90.4% at pH 3.0 with log K 8.26), while those with a 1:1 stoichiometry, which show much lower abundance/stability are: LQH_2 (36.6% at pH 2.0 with log K 5.18) and LQH (25.4% at pH 4.4 with log K 6.03).

In order to evaluate the stoichiometry and stability of Co^{2+}, Ni^{2+}, Cd^{2+}, and Cr^{3+} complexes with L and Q, known concentrations of L, Q, and their 1:1 mixture were also titrated in the presence of the metal ions and the resulting pH titration profiles in the presence of Co^{2+}, Ni^{2+}, Cd^{2+}, and Cr^{3+} species are also shown in Fig. 17(a) and (b). As can be seen, the potentiometric titration curves are depressed considerably in the presence of the metal ions. The extent of depression obviously depends both on the stoichiometries of the resulting complexes and the ability of the metal ions to bind the ligand components. The evaluated distribution diagrams for proton transfer interaction between L and Q are shown in Fig. 18, and those for the metal ion complexation with L and Q are presented in Fig. 19 and 20, respectively.

The cumulative stability constants, β_{mlqh}, are defined by eqn (1) (charges are omitted for simplicity):

$$m\mathrm{M} + l\mathrm{L} + q\mathrm{Q} + h\mathrm{H} \rightleftharpoons \mathrm{M}_m\mathrm{L}_l\mathrm{Q}_q\mathrm{H}_h \quad \beta_{mlqh}$$

$$\beta_{mlqh} = [\mathrm{M}_m\mathrm{L}_l\mathrm{Q}_q\mathrm{H}_h]/[\mathrm{M}]^m[\mathrm{L}]^l[\mathrm{Q}]^q[\mathrm{H}]^h \quad (1)$$

where M is metal ion, L is H_2hypydc, Q is 9a-Acr, H is proton, and m, l, q, and h are the respective stoichiometric coefficients. Since the activity coefficients of ligands and their complexes are unknown, the β_{mlqh} values are defined in terms of concentrations. The errors are minimized by the use of a high constant ionic strength of 0.1 M and low ligand concentrations (on the order of 10^{-3} M). The potentiometric pH titration curves of H_2hypydc, 9a-Acr, and their 1:1 mixture in the presence of metal ions were fitted by the program BEST.[30]

As is clear from Table 5 and Fig. 19 and 20, in the case of complexation of Co^{2+}, Ni^{2+}, Cd^{2+}, and Cr^{3+} ions with L, the most likely species with an abundance of 90% and higher, for Co^{2+} are CoL_2 (pH 3.5), $CoL_2(OH)_2$ (pH 11.9); for Ni^{2+} are NiL_2H_2 (pH 2.0), NiL_2 (pH 4.5), $NiL_2(OH)_3$ (pH 11.9); for Cd^{2+} are CdL_2H_2 (pH 2.0), CdL_2 (pH 4.4), $CdL_2(OH)_2$ (pH 6.7), $CdL_2(OH)_3$ (pH 11.9); for Cr^{3+} are CrL_2H (pH 3.2), CrL_2OH (pH 5.4), $CrL_2(OH)_3$ (pH 11.9). In the case of Q, those for Co^{2+} are CoQ_2 (pH 7.6), $CoQ_2(OH)_2$ (pH 11.9); for Ni^{2+} is NiQ_2H (pH 6.3); for Cd^{2+} are CdQ_2H (pH 4.4), $CdQ_2(OH)_2$ (pH 11.9); for Cr^{3+} is CrL_2H (pH 2.8).

Fig. 21(a) shows the pH potentiometric curves for the titration of a 1:1 mixture of the L–Q proton-transfer system, in the absence and presence of Co^{2+}, Ni^{2+}, Cd^{2+}, and Cr^{3+} ions, in a 50% methanol–50% water mixture with a standard LiOH solution. As clearly seen from Fig. 21, the potentiometric titration curves are depressed significantly in the presence of the metal ions studied. The sample species distribution diagrams for the L + Q mixture in the presence of Co^{2+}, Ni^{2+}, Cd^{2+}, and Cr^{3+} ions are illustrated in Fig. 21(b) to (e), respectively. The L, Q, and their protonated forms are not shown in the distribution curves of metal complexes for simplicity. The cumulative stability constants of different species involved in the distribution diagrams shown in Fig. 21, the corresponding pH titration curves determined with the program BEST,

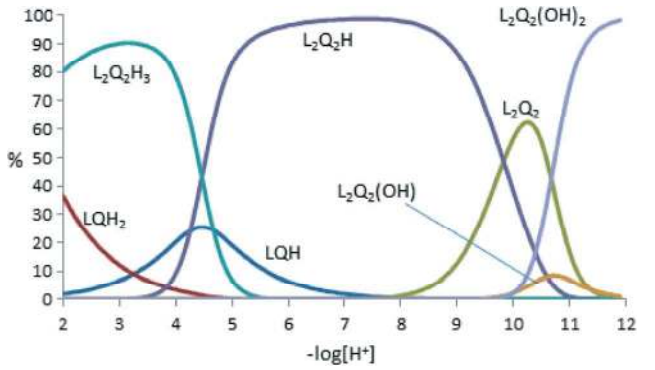

Fig. 18 Distribution diagram of proton transfer interaction between 9a-Acr (Q) and hypydc (L).

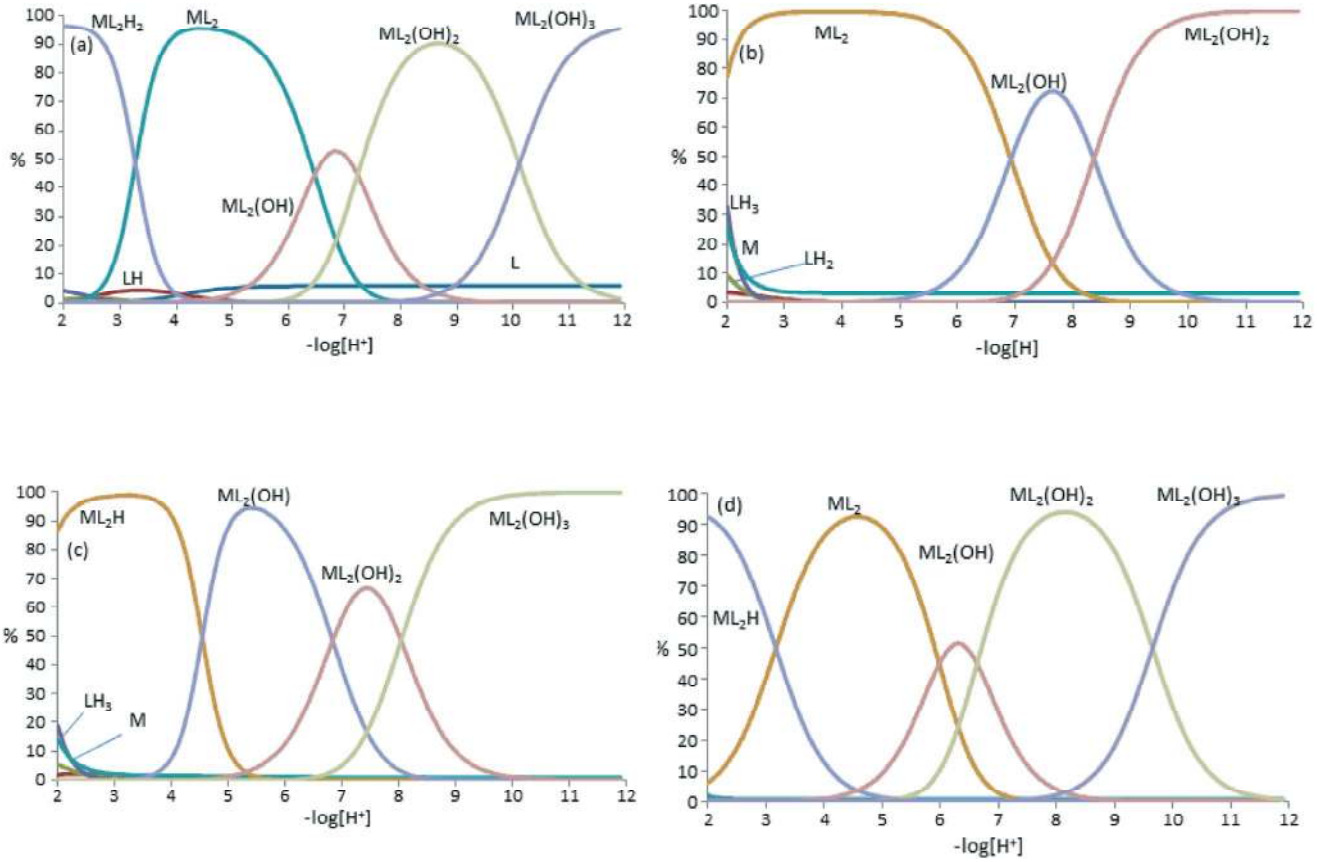

Fig. 19 Distribution diagrams of hypydc(L)–M^{n+} binary systems: M^{n+} = Cd^{2+} (a), Co^{2+} (b), Cr^{3+} (c), and Ni^{2+} (d).

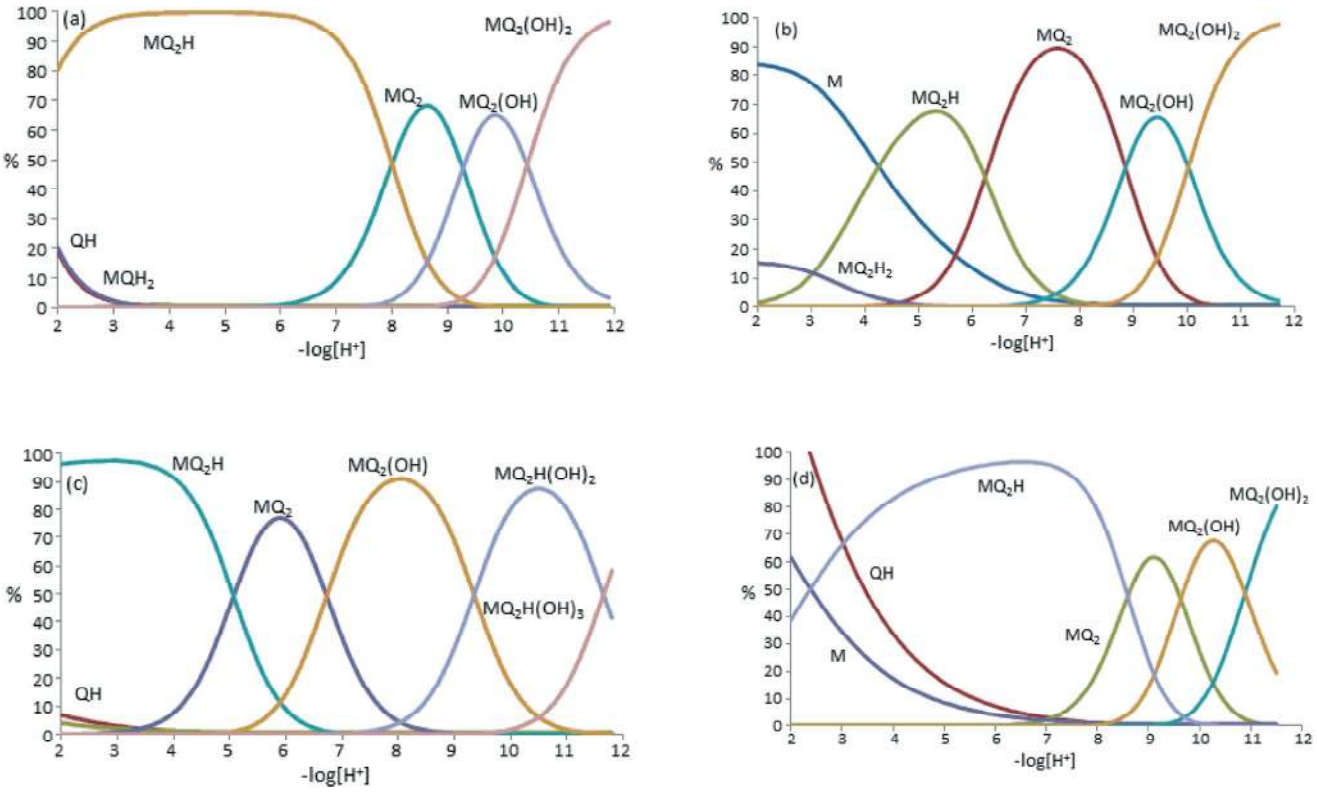

Fig. 20 Distribution diagrams of 9a-Acr(Q)–M^{n+} binary systems: M^{n+} = Cd^{2+} (a), Co^{2+} (b), Cr^{3+} (c), and Ni^{2+} (d).

Table 5 Overall stability constants of H_2hypydc–9a-Acr–M^{r+} ($l/q/m$) binary and ternary systems in a 50% methanol–50% water t at 25 °C and μ = 0.1 M $NaNO_3$

System	m	l	q	h	log β	Max%	pH
Cd–hypydc	1	2	0	0	17.31	95.6	4.4
	1	2	0	2	23.83	96.6	2
	1	2	0	−1	10.85	52.8	6.8
	1	2	0	−2	3.63	90.2	6.7
	1	2	0	−3	−6.48	95.4	11.9
Co–hypydc	1	2	0	0	8.02	99.6	3.3–4.5
	1	2	0	−1	1.1	72.2	7.6
	1	2	0	−2	−7.25	99.8	11.9
Cr–hypydc	1	2	0	1	10.82	98.8	3.2
	1	2	0	−1	1.75	94.4	5.4
	1	2	0	−2	−5.08	66.6	7.4
	1	2	0	−3	−13.12	99.8	11.9
Ni–hypydc	1	2	0	0	10.7	92.6	4.5
	1	2	0	1	13.86	92.4	2
	1	2	0	−1	4.72	51.4	8.3
	1	2	0	−2	−1.91	94	8.1
	1	2	0	−3	−11.56	99.8	11.9
Cd–9a-Acr	1	0	1	2	14.85	20.2	2
	1	0	2	0	13.62	68.2	8.6
	1	0	2	1	21.6	99.8	4.4–5.1
	1	0	2	−1	4.34	65	9.9
	1	0	2	−2	−6.08	96.6	11.9
Co–9a-Acr	1	0	2	0	8.45	89.6	7.6
	1	0	2	1	14.68	67.8	5.3
	1	0	2	2	17.71	15.2	2
	1	0	2	−1	−0.3904	65.6	9.4
	1	0	2	−2	−10.41	98.6	11.9
Cr–9a-Acr	1	0	2	0	15.51	77	5.9
	1	0	2	1	20.57	97.6	2.8
	1	0	2	−1	8.79	91	9
	1	0	2	−2	−0.552	87.6	10.5
	1	0	2	−3	−12.2	63.8	11.9
Ni–9a-Acr	1	0	2	0	7.92	61.8	9.1
	1	0	2	1	16.51	96.6	6.3
	1	0	2	−1	−1.71	67.6	10.3
	1	0	2	−2	−12.59	80.2	11.9
Cd–hypydc–9a-Acr	1	2	2	0	29.77	91.8	8.8
	1	2	2	1	36.98	76.8	6.4
	1	2	2	2	42.52	85.4	4.4
	1	2	2	3	45.85	93.8	2
Co–hypydc–9a-Acr	1	2	2	0	23.6	84.8	7.5
	1	2	2	1	30	66.4	5.8
	1	2	2	2	35.17	96.2	3.2
	1	2	2	−1	15.05	81.6	9.7
	1	2	2	−2	4.54	94.6	11.9
Cr–hypydc–9a-Acr	1	2	1	0	15.25	17.8	4.3
	1	2	1	−1	10.08	<10	4.7
	1	2	1	−3	1.52	51	6.3–7.9
	1	2	1	−4	−8.82	92	11.9
Ni–hypydc–9a-Acr	1	2	2	0	28.15	59.4	7
	1	2	2	1	34.62	99.8	3.2–3.5
	1	2	2	−1	20.74	87.4	8.5
	1	2	2	−2	11.03	49.6	10
	1	2	2	−3	0.72	97.2	11.9

using eqn (1), and the resulting stability values in a 50% methanol–50% water mixture for the most likely species are also included in Table 5. The titration data of L + Q system show that there is no detectable interaction between L and Q, in the presence of the metal ions studied.

Fig. 21(b) to (e) and data given in Table 5 indicated the formation of a variety of ternary complexes between Co^{2+}, Ni^{2+}, Cd^{2+}, and Cr^{3+} ions and the L–Q proton-transfer system at different ranges of pH. The predominant species for Co^{2+} are $CoL_2Q_2H_2$ (96.2% at pH 3.2) and $CoL_2Q_2(OH)_2$ (94.6% at pH 11.9); for Ni^{2+} are NiL_2Q_2H (99.8% at pH 3.2–3.5) and NiL_2Q_2OH (87.4% at pH 8.5); for Cd^{2+} are $CdL_2Q_2H_3$ (93.8% at pH 2.0) and CdL_2Q_2 (91.8% at pH 8.8); for Cr^{3+} is $CrL_2Q_2(OH)_4$ (92.0% at pH 11.9). It is interesting to note that

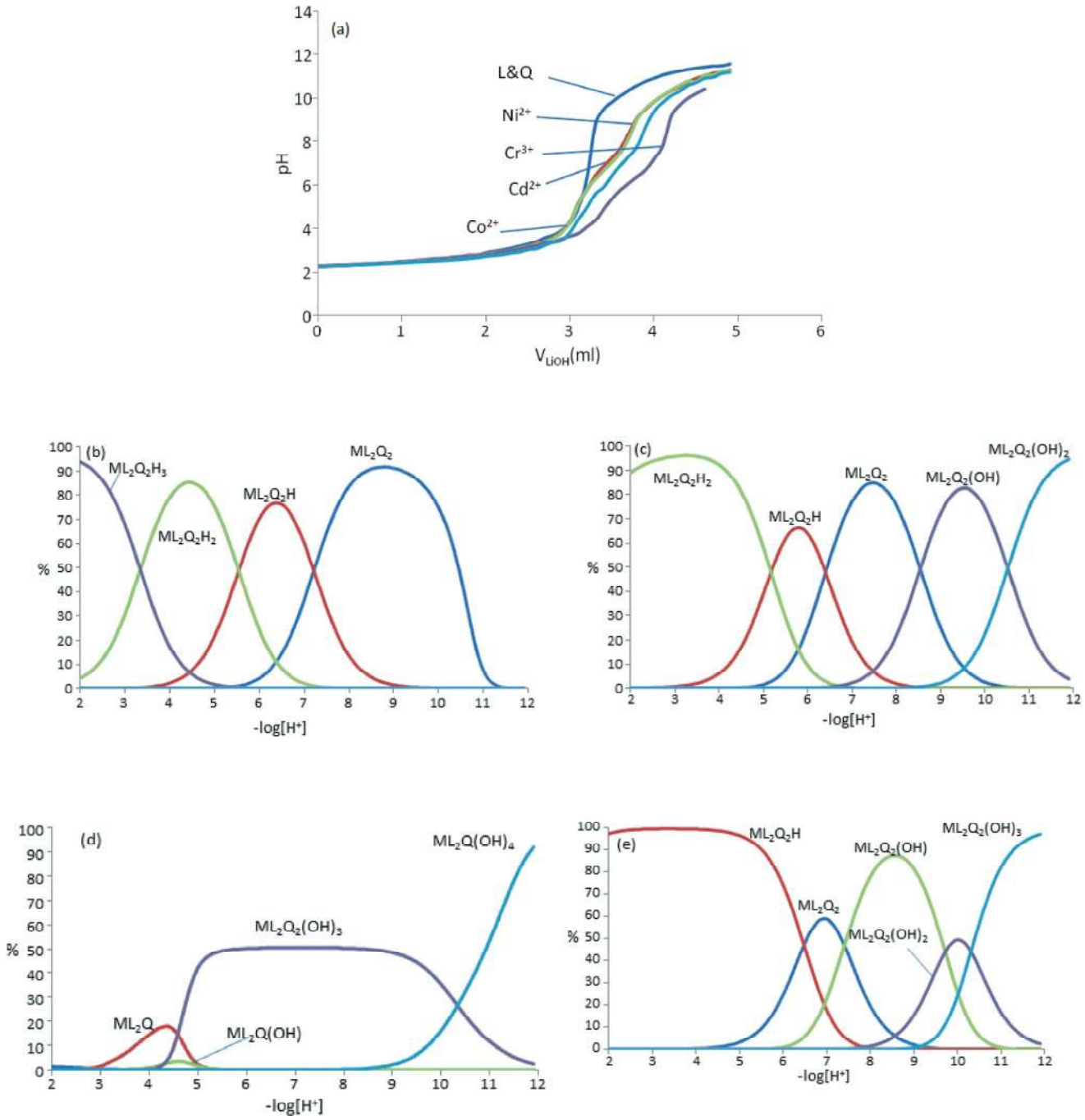

Fig. 21 Potentiometric titration curves of hypydc + 9a-acr in the absence and presence of Co^{2+}, Ni^{2+} Cd^{2+}, and Cr^{3+} ions with 0.059 M LiOH in a 50% methanol–50% water solvent at 25 °C and μ = 0.1 M $NaNO_3$ (a), and distribution diagrams of hypydc (L)–9a-Acr (Q)–M'^{n+} ternary systems, where M'^{n+} = Cd^{2+} (b), Co^{2+} (c), Cr^{3+} (d), and Ni^{2+} (e).

the stoichiometries of some of the most abundant ternary complexes, existing in 50% methanol–50% water solution, are the same or very similar to those obtained for the corresponding isolated complexes in the solid state.

4. Concluding remarks

We have successfully synthesized and characterized four new proton-transfer compounds $(H9a\text{-}Acr)_2[Ni(hypydc)_2]\cdot 4H_2O$ (1), $(H9a\text{-}Acr)_2[Co(hypydc)_2]\cdot 3H_2O$ (2), $(H9a\text{-}Acr)[Cr(hypydc)_2]\cdot 3H_2O$ (3), and $(H9a\text{-}Acr)_2[Cd(hypydc)_2]\cdot 3H_2O$ (4). The chelidamic ligand acts as a tridentate ligand through two O atoms of the carboxylate groups and one N atom of the pyridine ring. In all compounds strong hydrogen bonds between anions, cations, and lattice water molecules together with a variety of π···π interactions play an important role in the construction of the 3-D supramolecular frameworks. Different types of interactions involving the lattice water molecules are observed that

are crucial for the formation of the 2-D anionic layers. In 3, a totally different 3-D architecture has been found where instead of layers, a grid is formed caused by the action of π^-–π^- stacking interactions instead of the π^-–π^+ and π^-–π^- interactions observed in the rest of the compounds. The smaller *trans* N–M–N angle observed in 3 has been analyzed using DFT calculations. As a result, we have concluded that in the Co^{2+} and Ni^{2-} complexes the bending of the *trans* N–M–N angle from 180° to 165° has a negligible energetic cost, in agreement with the angle observed experimentally for the Co complex. In addition, we have evaluated the different nature of the π^+–π^- and π^-–π^- stacking interactions which play a key role in the final geometry of compounds 1–4. Finally, in a solution study, the protonation constants of H_2hypydc (L) and 9a-Acr (Q), the equilibrium constants of the L–Q proton-transfer system and the stoichiometry and stability of complexation of this system with Co^{2+}, Ni^{2+}, Cd^{2+}, and Cr^{3+} ions in a 50% methanol–50% water mixture were investigated by potentiometric pH titrations. The stoichiometry of most of the complexed species in solution was found to be very similar to that obtained in the crystalline metal ion complexes.

Acknowledgements

HEH and MM wish to thank to the Ferdowsi University of Mashhad for financial support of this article (grant no. 19023/3). This work was supported by the DGICYT of Spain (CTQ2011-27512/BQU and CONSOLIDER INGENIO CSD2010-00065, FEDER funds) and the Direcció General de Recerca i Innovació del Govern Balear (project 23/2011, FEDER funds). JTM thanks the Chemistry Department of Tulane University for support of the Tulane Crystallography Laboratory.

References

1 E. F. Caldin and V. Gold, *Proton-transfer Reactions*, Chapman and Hall, London, 1975.
2 *Theoretical Treatments of Hydrogen Bonding*, ed. D. Hadzi, John Wiley & Sons Ltd., Chichester, 1997.
3 N. S. Golubev, I. G. Shenderovich, S. N. Smirnov, G. S. Denisov and H. H. Limbach, *Chem.–Eur. J.*, 1999, **5**, 492.
4 S. S. Smirnov, N. S. Golubev, G. S. Denisov, H. Benedict, P. Schah-Mohammedi and H. H. Limbach, *J. Am. Chem. Soc.*, 1996, **118**, 4094.
5 H. Fu and A. Fu, *THEOCHEM*, 2007, **818**, 163.
6 (*a*) M. Mirzaei, H. Aghabozorg and H. Eshtiagh-Hosseini, *J. Iran. Chem. Soc.*, 2012, **8**, 580, and references therein, (*b*) H. Eshtiagh-Hosseini, M. Mirzaei and N. Alfi, *Review on Proton Transfer Metal Complexes*, Lambert Academic Publishing GmbH & Co. KG., First edn, 2012.
7 (*a*) D. L. Boger, J. Hong, M. Hikota and M. Ishida, *J. Am. Chem. Soc.*, 1999, **121**, 2471; (*b*) S. W. Ng, *J. Organomet. Chem.*, 1999, **12**, 585; (*c*) Y. Nakatsuji, J. S. Bradshaw, P. K. Tse, G. Arena, B. E. Wilson, N. K. Wilson, N. K. Dalley and R. M. Izatt, *J. Chem. Soc., Chem. Commun.*, 1985, 749; (*d*) T. Fessmann and J. D. Kilburn, *Angew. Chem., Int. Ed.*, 1999, **38**, 1993; (*e*) G. J. Bridger, R. T. Skerlj, S. Padmanabhan, S. A. Martellucci, G. W. Henson, S. Struyf, M. Witvrouw and D. Schols, *J. Med. Chem.*, 1999, **42**, 3971; (*f*) M. Searcey, S. McClean, B. Madden, A. T. McGown and L. P. G. Wakelin, *Anti-Cancer Drug Des.*, 1998, **13**, 837.
8 M. Mirzaei, V. Lippolis, H. Eshtiagh-Hosseini and M. Mahjoobizadeh, *Acta Crystallogr., Sect. C: Cryst. Struct. Commun.*, 2011, **68**, m7.
9 H. Aghabozorg, N. Firoozi, L. Roshan, H. Eshtiagh-Hosseini, A. R. Salimi, M. Mirzaei, M. Ghanbari, M. Shamsipur and M. Ghadermazi, *J. Iran. Chem. Soc.*, 2012, **8**, 992.
10 H. Eshtiagh-Hosseini and M. Mirzaei, *Mendeleev Commun.*, 2012, **22**, 323.
11 G.-W. Zhou, G.-C. Guo, B. Liu, M.-S. Wang, L.-Z. Cai, G.-H. Guo and J.-S. Huang, *Acta Crystallogr., Sect. E: Struct. Rep. Online*, 2003, **59**, m926.
12 M. Ramos Silva, E. Motyeian, H. Aghabozorg and M. Ghadermazi, *Acta Crystallogr., Sect. E: Struct. Rep. Online*, 2008, **64**, m1173.
13 H. Aghabozorg, E. Motyeian, J. A. Gharamaleki, J. Soleimanne-jad, M. Ghadermazi and E. S. Sharon, *Acta Crystallogr., Sect. E: Struct. Rep. Online*, 2008, **64**, m144.
14 H. Aghabozorg, N. Ilaie, M. Heidari, F. Manteghi and H. Pasdar, *Acta Crystallogr., Sect. E: Struct. Rep. Online*, 2008, **64**, m1351.
15 H. Aghabozorg, E. Motyeian, J. Soleimannejad, M. Ghadermazi and J. A. Gharamaleki, *Acta Crystallogr., Sect. E: Struct. Rep. Online*, 2008, **64**, m252.
16 (*a*) M. Mirzaei, H. Eshtiagh-Hosseini, Z. Karrabi and B. Notash, *Acta Crystallogr., Sect. C: Cryst. Struct. Commun.*, 2013, **69**, m1140; (*b*) H. Aghabozorg, N. Firoozi, L. Roshan, H. Eshtiagh-Hosseini, A. R. Salimi, M. Mirzaei, M. Ghanbari, M. Shamsipur and M. Ghadermazi, *J. Iran. Chem. Soc.*, 2012, **8**, 992.
17 J. P. Zou, M. H. Chen, S. L. Luo, X. H. Tang, Z. Q. Xiong and Q. Peng, *Inorg. Chim. Acta*, 2011, **373**, 243.
18 Z. Derikvand, A. Nemati, A. Shokrollahi and F. Zarghampour, *Inorg. Chim. Acta*, 2012, **392**, 362.
19 J.-P. Zou, S. C. Dai, W.-T. Guan, H.-B. Yang, Y.-F. Feng and X.-B. Luo, *J. Coord. Chem.*, 2012, **65**, 2877.
20 Z. Derikvand, M. M. Olmstead, B. Q. Mercado, A. Shokrollahi and M. Shahryari, *Inorg. Chim. Acta*, 2013, **406**, 256.
21 S. L. Wu, J. P. Zou, M. H. Chen, H. B. Yang, M. J. Li, X. B. Luo, F. Luo, M. F. Wu and G. C. Guo, *Polyhedron*, 2012, **48**, 58.
22 J. P. Zou, S. L. Luo, M. J. Li, X. H. Tang, Q. J. Xing, Q. Peng and G. C. Guo, *Polyhedron*, 2010, **29**, 2674.
23 *APEX2, Bruker-AXS*, Madison, WI, 2012.
24 *SAINT, Bruker-AXS*, Madison, WI, 2012.
25 *SADABS, Bruker-AXS*, Madison, WI, 2012.
26 G. M. Sheldrick, *Acta Crystallogr., Sect. A: Found. Crystallogr.*, 2008, **64**, 112.
27 R. Ahlrichs, M. Bär, M. Hacer, H. Horn and C. Kömel, *Chem. Phys. Lett.*, 1989, **162**, 165.

28 S. Grimme, S. Ehrlich and L. Goerigk, *J. Comput. Chem.*, 2011, **32**, 1456–1465.
29 S Rondinini, T Longhi, P. R. Mussini and T. Mussini, *Pure Appl. Chem.*, 1987, **59**, 1693.
30 E. Martell and R.-J. Motekaitis, *Determination and Use of Stability Constants*, VCH, New York, second edn, 1992.
31 G. Schwarzenbach and H. Flaschka, *Complexometric Titrations*, Methuen, London, 1969.
32 K. Nakamoto, *Infrared and Raman Spectra of Inorganic and Coordination Compounds, Part B*, Wiley, New York, 5th edn, 1997.
33 S. K. Seth, P. Manna, N. J. Singh, M. Mitra, A. D. Jana, A. Das, S. R. Choudhury, T. Kar, S. Mukhopadhyay and K. S. Kim, *CrystEngComm*, 2013, **15**, 1285.
34 A. Das, S. R. Choudhury, B. Dey, S. K. Yalamanchili, M. Helliwell, P. Gamez, S. Mukhopadhyay, C. Estarellas and A. Frontera, *J. Phys. Chem. B*, 2010, **114**, 4998.
35 H. Aghabozorg, L. Roshan, N. Firoozi, M. Ghadermazi and S. Bagheri, *Acta Crystallogr., Sect. E: Struct. Rep. Online*, 2008, **64**, m1208.
36 M. Rafizadeh, Z. Derikvand and A. Nemati, *Acta Crystallogr., Sect. E: Struct. Rep. Online*, 2008, **64**, m1300.
37 Z. Derikvand, A. Nemati, A. Sholkollahi and F. Zaeghampour, *Inorg. Chim. Acta*, 2012, **392**, 362.
38 M. Rafizadeh, A. Nemati and Z. Derikvand, *Acta Crystallogr., Sect. E: Struct. Rep. Online*, 2008, **64**, m1298.
39 M. Ghadermazi, F. Manteghi and H. Aghabozorg, *Acta Crystallogr., Sect. E: Struct. Rep. Online*, 2009, **65**, m1374.